UNIVERSITY OF CALIFORNIA MERCED

DEVELOPMENT AND APPLICATION OF WRF3.3-CLM4CROP TO STUDY OF AGRICULTURE - CLIMATE INTERACTION

A dissertation submitted in partial satisfaction of the requirements for the degree Doctor of Philosophy

in

Environmental Systems

by

Yaqiong Lu

Committee in charge:

Dr. Lara M. Kueppers, Chair
Dr. J. Elliott Campbell
Dr. Jiming Jin

The dissertation of Yaqiong Lu is approved, and it is accepted in quality and form for publication on microfilm and electronically:

_____

Dr. J. Elliott Campbell Date

_____

Dr. Jiming Jin Date

_____

Dr. Lara M. Kueppers, Chair Date

University of California, Merced
2013

TABLE OF CONTENTS

LIST OF FIGURES

LIST OF TABLES

CURRICULUM VITAE

Education:

2005 B.S. Major: Atmospheric Sciences, Chengdu University of Information and Technology, Chengdu, China.
2008 M.S. Major: Physical Geography, Institute of Tibetan Plateau Research, Chinese Academy of Sciences.
2013 Ph.D. Major: Environmental Sciences, University of California, Merced.

Research interests:

Regional climate modeling
Land surface modeling
Agriculture and climate interaction
Land use change effects on climate

Publications:

Lu, Y. and L. Kueppers. Surface energy partitioning over our dominant vegetation types in a coupled regional climate model (WRF3.0-CLM3.5) across the United States. Journal of Geophysical Research, atmosphere, vol. 117 ,D06111, 2012

ACKNOWLEDGEMENTS

I would like to first thank my committee chair, Professor L.M. Kueppers for all the five years mentoring and supporting. You set up an excellent example as a woman in pursue of scientific career. Your broad knowledge in sciences, smart thoughts, collaborative working style have profound influence on me. I also like to thank my committee members, Professor J. Jin and Jr. E. Campbell for your great suggestions on my dissertation. Without the advice and help from my committee, this dissertation would not been possible. Let me thank Professor J. Jin again for the help on the climate model coupling. I learned important skill on how to couple the land surface model into the regional climate model step by step. I thank Professor A. Westerling for teaching the class Applied Climatology, where I learned the powerful tool R that I used to process and analyze the observation data. I thank Joseph Norris for thousands times assistant on installing the software and trouble shooting on the cluster. Let me thank University of California, Merced. Without the summer fellowships and Teaching Assistant position, my PhD study would not been such smoothly. I thank the useful feedbacks I received from my group, Kaitlin Lubetkin, Miguel Fernandez, Daniel Winkler, Andrew Moyes, and Meredith Jabis. In the end, I thank my family for the understanding and support of my PhD study.

ABSTRACT

DEVELOPMENT AND APPLICATION OF WRF3.3-CLM4CROP TO STUDY OF AGRICULTURE - CLIMATE INTERACTION
by
Yaqiong Lu
Doctor of Philogophy
University of California, Merced
Dr. Lara M. Kueppers, Chair

Accurate representation of surface energy partitioning is crucial for studying land surface processes and the climatic influence of land cover and land use change using coupled climate-land surface models. A critical question for these models, especially for newly coupled ones, is whether they can adequately distinguish differences in surface energy partitioning among different vegetation types. In the first chapter, I evaluated three years (2004-2006) of surface energy partitioning and surface climate over four dominant vegetation types (cropland, grassland, needleleaf evergreen forest, broadleaf deciduous forest) across the United States in a recently coupled regional climate model (WRF3-CLM3.5) by comparing model output to observations (AmeriFlux, CERES, and PRISM data) and to standard WRF output. I found that WRF3-CLM3.5 can capture the seasonal pattern in energy partitioning for needleleaf evergreen forest, but needs improvements in cropland, grassland and broadleaf deciduous forest.

To extend the capability of the regional climate model in studying the interaction of climate and agriculture, in the second chapter, I coupled a version of the Community Land Model that includes crop growth and management (CLM4crop) into the Weather Research and Forecasting model (WRF) and evaluated against multiple observations. The evaluation showed that although the model with dynamic crops overestimated LAI and growing season length, interannual variability in LAI was improved relative to a model with prescribed crop LAI and growth period, which has no environmental sensitivity. Improvements in climate variables were limited by an overall model dry bias. However, with addition of an irrigation scheme, soil moisture and energy fluxes were largely improved at irrigated sites. With this improved model, I further investigated whether the dynamic crop growth influenced the irrigation effects on climate. With prescribed crop LAI and growth, irrigation effects on climate were under-predicted in moderately irrigated regions. Moreover, relative to the dynamic crop growth version, the prescribed crop growth model underestimated irrigation water use and simulated much higher soil evaporation.

The third chapter is an application of the coupled model in studying the irrigation effects on heat waves. A potential decline in irrigation due to groundwater depletion would not only directly affect agriculture, but also could potentially alter surface climate. In this study I investigated how irrigation affects heat wave frequency, duration, and intensity using fifteen heat wave indices and a regional climate model. Across all indices,

irrigation reduced heat wave frequency and duration, but increased intensity. Irrigation effects on heat waves are statistically significant over irrigated cropland and but not significant for non-irrigated regions. The magnitude of effect varies by index and is more sensitive to the choice of temperature metric than to the choice of temperature threshold. Regions experiencing strong groundwater depletion, such as the southern high plains, may suffer more and longer heat waves with reduced irrigation.

Overall, my research confirmed the dynamic crop growth model and irrigation are important in studying the agriculture and climate interaction. The research on irrigation effects, as well as on weather and climate prediction, should include dynamic crop growth and realistic irrigation schemes to better capture land surface effects in agricultural regions.

Introduction

Although the response of agricultural systems to climate is drawing considerable attention because of the potential for a global food crisis, current understanding of how climate affect agricultural production is highly uncertain since the feedbacks between them are not well studied. Agricultural systems are highly vulnerable to climate variability, where the area suitable for agriculture, the length of growing seasons and yield potentials are expected to change under warming scenarios [*IPCC*, 2007]. In addition, crop growth alters some important physical climate forcings, such as latent heat flux, shortwave radiation, longwave radiation and soil moisture. This two-way interaction is often referred to as a feedback, describing a nonlinear cycle between two systems. Clarifying the importance of these feedbacks could improve regional climate simulations in agriculturally intensive areas and enable better prediction of crop production.

Variability in atmospheric CO_2, temperature and precipitation highly affect agricultural production. The elevated CO2 could increase photosynthetic productivity [*Aoki and Yabuki*, 1977; *Cooper and Brun*, 1967; *Moss*, 1962] and therefore lead to an increase of yield. Amthor [2003] reviewed the previous observations and suggested doubling CO_2 could increase the yield by 31% in average. At the same time, double CO_2 could lead to 34% reduction of transpiration and double water use efficiency [*Kimball and Idso*, 1983]. In one study, increase in variability of temperature and precipitation resulted in significant increases in yield variability and crop failures [*Mearns et al.*, 1992]. Warming by 2-4 ^{o}C could results in substantial shortening of the growing season, and change of crop calendar, particularly in winter [*Butterfield and Morison*, 1992]. Furthermore, increasing temperature and precipitation could have different impacts on yields for different crops. For example, a simulation study indicated potato production was increasing while wheat and faba bean was decreasing with increased temperature, and increasing of precipitation had no effect on the yield of potatoes or spring wheat, but could reducing winter wheat yield [*Peiris et al.*, 1996].

Meanwhile, agriculture also affects climate by altering the surface energy, water, and carbon cycle. Cropland plays a very important biogeophysical role in changing climate [*Feddema et al.*, 2005; *Foley et al.*, 2005; *Pitman et al.*, 1999]. Agricultural expansion in business as usual (A2) scenario results in significant additional warming over the Amazon and cooling of the upper air column and nearby oceans [*Feddema et al.*, 2005]. Crops alter the small-scale boundary layer structure [*Adegoke et al.*, 2007], such as surface wind and boundary layer height, by increasing canopy height during the growth process. Compared to natural vegetation, cropland has higher albedo that alters the energy budget when converting between forest and cropland [*Bonan*, 2008; *Oleson et al.*, 2004]. Cropland also alters the water cycle. Both field observations and modeling have shown that conversion of forest to cropland can reduce evaportranspiration and precipitation at the regional scale [*Sampaio et al.*, 2007]. Moreover, agriculture and associated management practices were found to affect the carbon cycle [*Lal*, 2004]. Global simulation indicates a 24% reduction in global vegetation carbon due to

agriculture [*Bondeau et al.*, 2007a]. Growing biofuel crops at previously natural vegetation land could increase greenhouse gas emissions by 50% [*Searchinger et al.*, 2008].

Both observations and numerical modeling are used to study climate effects on agriculture. Laboratory studies using growth chambers and greenhouses showed elevated CO2 could increase net photosynthesis [*Aoki and Yabuki*, 1977; *Cooper and Brun*, 1967; *Moss*, 1962]. These stuides had a short period measurements and the high CO2 concentrations were not realistic. Free air CO2 enrichment experiments [*Ainsworth and Long*, 2005; *Ainsworth et al.*, 2002; *Long et al.*, 2006] using long term observation confirmed some chamber experiment results that trees were more responsive than herbaceous species to elevated CO2, but crop grain yields increased far less than in previous enclosed studies. Regression models [*Rosenberg*, 1982] also have been employed to study how climate affects crop yield and this method is still widely used today [*Diffenbaugh et al.*, 2012; *Lobell et al.*, 2008b]. Finally, crop growth models (such as CERES [*Lizaso and Ritchie*, 1997; *Ritchie and Otter*, 1985], SOYGRO[*Wilkerson et al.*, 1983], EPIC [*Easterling et al.*, 1992; *Rosenberg et al.*, 1992], AFRC-Wheat [*Butterfield and Morison*, 1992]) enable yield prediction and hazard prevention.

Climate models are widely used to study the effects of agriculture on climate. Climate models (called general circulation models initially) were first developed for numerical weather prediction in the 1950s, and had a very coarse resolution only contained atmosphere circulation. In 1960-1970s, the climate model included both ocean and atmosphere circulations. In 1980-2000s, the development of regional climate model and sub-grid physical process model (land surface model, boundary layer model, microphysics model, cumulus model, etc.) not only aim to improve the forecasting skill but also to study the climate change. In climate model, the land surface model provides sensible, latent, and momentum flux for atmosphere model to solve the atmospheric equations. The potential climate sensitivity to land use change is determined by the difference between two simulations (control and sensitive simulations) that differ only in land use. A key determinant in accuracy of such research is how well the land surface model simulates the surface energy fluxes (i.e., sensible heat flux, latent heat flux, and ground heat flux). The development of land surface model is getting more and more comprehensive to reflect the reality [*Bonan*, 2008]. Early land surface models represented the physical processes using simple parameterizations. For example, the soil hydrology was represented as a bucket, which could hold some maximum amount of water filled by precipitation, with the excess water becoming runoff. Currently, most land surface models include all the major parameterizations, such as vegetation photosynthesis and conductance, snow accumulation and melting, radiation transfer, and turbulence processes above and within the canopy, etc. Moreover, some advanced land surface models include the carbon cycle and dynamic vegetation growth.

Coupling a land surface model that incorporates dynamic crop growth into a climate model enables simulation of the two-way interactions between climate and crop growth. Recent work incorporating crop growth models into climate models has revealed that dynamic crop growth strongly influences regional climate patterns by altering land

surface water and energy exchange [*Bondeau et al.*, 2007b; *Levis et al.*, 2012; *Liang et al.*, 2012; *Lu et al.*, 2001; *Osborne et al.*, 2007; *Tsvetsinskaya et al.*, 2000; *Xu et al.*, 2005]. Most of these studies have not rigorously evaluated results against observations of climate and crop variables. Further, interactions between crop growth and irrigation effects on climate are not well examined.

The aim of the work is to improve a regional climate model by incorporating a land surface model that simulates dynamic crop growth. Particularly, my work focuses on the improvement and evaluation of the Weather Research and Forecasting Model (WRF3.3) with updated Community Land Model (CLM4), a dynamic crop growth model, and an irrigation scheme. As the next-generation mesoscale numerical model, the standard version of WRF includes relatively simple land surface schemes, which potentially constrain model applications for studying the land surface and ecosystem-atmosphere feedbacks. By adding the CLM into WRF, I expected an improvement in surface energy flux simulations. Therefore, I first validated the performance for the surface energy fluxes for four vegetation types across the continental of United States in the first chapter [*Lu and Kueppers*, 2012]. Since one problem in this model was related to the low crop LAI bias and lack of irrigation, I further incorporated the dynamic crop growth model and irrigation into a new version (WRF3.3-CLM4crop). I evaluated the crop growth and climate variables in the new version and the influence of dynamic crop growth on irrigation effects was quantified. In the third chapter, I used the coupled model to study irrigation effects on heat wave frequency, duration, and intensity.

CHAPTER 1

Surface energy partitioning over four dominant vegetation types across the United States in a coupled regional climate model (WRF3-CLM3.5)

Introduction

A large number of observational and modeling studies have confirmed that the land surface plays a key role in weather and climate [*Feddema et al.*, 2005; *Kalnay and Cai*, 2003; *Pielke et al.*, 2002; *Pielke et al.*, 2007; *Pitman et al.*, 1999; *Seneviratne et al.*, 2006]. The land surface influences the atmosphere through exchange of energy, momentum, water, and CO_2 and other trace gases across the atmospheric boundary layer [*Bounoua et al.*, 2002; *Cox et al.*, 2000]. Conversion from one land cover to another can alter albedo, surface hydrology, boundary layer roughness length, and therefore surface energy partitioning. Moreover, various types of land cover changes can generate quite different climate changes. For instance, conversion of Amazon forest to pasture has significantly increased surface temperature and reduced evaporation and precipitation [*Malhi et al.*, 2008; *Shukla et al.*, 1990], while replacing natural grassland with irrigated cropland has introduced much more evaportranspiration and reduced surface temperature [*Bonfils and Lobell*, 2007; *Diffenbaugh*, 2009; *Kueppers et al.*, 2007a; *Lobell et al.*, 2009]. Even in the absence of irrigation, studies confirm that soil moisture has strong leverage on energy flux partitioning at the surface [*Dirmeyer et al.*, 2000; *Guo et al.*, 2006; *Koster et al.*, 2004].

As climate models become a primary tool for studying the atmospheric role of land surface processes, a question for current climate models is whether they can adequately distinguish and accurately simulate surface energy partitioning over different vegetation types. Plants contribute a large fraction of latent heat flux through evaporation of water from leaf surfaces and transpiration from deeper soil layers when stomata open during photosynthesis. Plants also affect net radiation by altering the surface albedo. A change in plant height can change the boundary layer turbulence by influencing surface roughness, and therefore the total energy exchange via latent and sensible heat fluxes [*Davin and de Noblet-Ducoudre*, 2010]. In most climate models, several important vegetation parameters (plant function type/vegetation type, leaf area index, stem area index, and canopy top/bottom height) are prescribed according to satellite observations and ground measurements. These parameters are not necessarily accurate at the site-scale due to the algorithm and validation methods used in retrieving satellite data or aggregating ground data [*Yang et al.*, 2006]. Validation of surface fluxes over different vegetation types can help identify deficiencies in key parameters and model formulations to target for improving model performance.

Increasing ground and satellite based observations of surface energy fluxes enable validation of energy partitioning in climate models. Ground based networks, such as FLUXNET [*Baldocchi et al.*, 2001] and SURFRAD [*Augustine et al.*, 2000] have helped to identify the source of radiation budgets and soil moisture errors [*Markovic et al.*, 2008; *Stockli et al.*, 2008; *Williams et al.*, 2009]. Satellite derived data, such as ISCCP [*Raschke*

et al., 2005] and CERES [*Wielicki et al.*, 1996] have also been used in model validation [*Su et al.*, 2010; *Wild and Roeckner*, 2006]. However, many of the validation studies have focused on site averages without considering the vegetation type [*Markovic et al.*, 2008] or a specific vegetation type in the domain, such as tundra in the arctic [*Lynch et al.*, 1999]. The validation of surface energy partitioning over a range of different vegetation types at continental scales has not been generally reported, even though observations suggest that surface energy partitioning varies considerably with vegetation type [*Wilson et al.*, 2002b].

The aim of this work is to examine energy partitioning and surface climate simulated by a recently coupled regional climate model, WRF3-CLM3.5, for four major vegetation types across the United States, and to identify the model's strengths and deficiencies to help prioritize model improvements. As the next-generation mesoscale numerical model, the standard version of WRF includes relatively simple land surface schemes, which potentially constrain model applications for studying the land surface and ecosystem-atmosphere feedbacks. The newly coupled model improved the surface process simulation in California [*Subin et al.*, 2011], but has not been validated at the continental scale. We used the standard version of the Weather Research and Forecasting (WRF) model version 3.0 [*Skamarock et al.*, 2008], AmeriFlux site observations [*Wofsy and Hollinger*, 1998], and CERES data [*Wielicki et al.*, 1996; *Young et al.*, 1998] to evaluate energy flux partitioning. We analyzed the bias in surface climate variables (daily maximum temperature, daily minimum temperature and precipitation) by comparing to PRISM datasets [*Di Luzio et al.*, 2008]. We focused on four dominant vegetation types with adequate representation in the AmeriFlux network (cropland, grassland, needleleaf evergreen forest and broadleaf deciduous forest).

Model and Data

The Community Land Model version 3.5 (CLM3.5) [*Oleson et al.*, 2008] has been coupled into The Weather Research and Forecasting Model version 3 (WRF3) [*Skamarock et al.*, 2008] in an effort to improve simulations of the effects of land cover and land use change on regional climate. Details of the coupling and model validation in California are documented elsewhere [*Subin et al.*, 2011], but will be briefly summarized here.

CLM3.5 represents the surface with five primary sub-grid land cover types (glacier, lake, wetland, urban[1], and vegetated) in each grid cell. The vegetated portion of a grid cell is further divided into patches of up to 4 of 16 plant functional types (PFTs) [*Bonan et al.*, 2002], each characterized by distinct physiological parameters [*Oleson et al.*, 2008]. The spatial distribution of plant function types and leaf area index are obtained from 1-km MODIS observations from 2001-2003. LAI is prescribed monthly and is updated daily by linearly interpolating between monthly values. The major improvements in CLM3.5 include new surface datasets [*Lawrence and Chase*, 2007], an improved canopy

[1] The urban sub-grid land cover type is not active in WRF3-CLM3.5

integration scheme [*Thornton and Zimmermann*, 2007], scaling of canopy interception [*Lawrence et al.*, 2007], a simple TOPMODEL-based model for surface and sub-surface runoff [*Niu et al.*, 2005], a simple groundwater model for determining water table depth [*Niu et al.*, 2007], and a new frozen soil scheme [*Niu and Yang*, 2006].

We set up two 5-year simulations (2002-2006) for standard WRF3.0.1 and WRF3-CLM3.5, which differed only in the land surface model (Noah vs. CLM). The Noah land surface model [*Chen and Dudhia*, 2001] has 4 soil layers (compared to 10 soil layers in CLM3.5) and only one vegetation type (instead of 4 PFTs in CLM3.5) for each grid cell. There is no separate treatment of shaded and sunlit canopy (CLM3.5 treats shaded and sunlit differently). The other physical packages used in our simulations include the YSU PBL scheme [*Hong et al.*, 2006], the Rapid Radiative Transfer longwave scheme [*Mlawer et al.*, 1997], the Goddard shortwave radiation parameterization[*Chou and Suarez*, 1994], the Purdue Lin bulk microphysics scheme [*Lin et al.*, 1983] and the Kain-Fritsch cumulus scheme [*Kain*, 2004]. These physical configurations yielded the best results for WRF3-CLM3.5 compared to 2 alternate configurations (one with Duhia short-wave scheme and one with Net Grell cumulus scheme, keeping other schemes the same). We used NCEP/DOE Reanalysis II data as boundary conditions for the period January 2002-December 2006. The simulations focused on the continental United States (U.S.) with 25 vertical layers and 50 km horizontal resolution. We interpolated (using the inverse distance weighting method) 0.5 deg CLM surface input data (including plant functional types, plant function type percent, leaf area index, and stem area index) into the model domain. For analysis, we removed 8 grid cells from the full perimeter of the domain as a buffer, which diminished the original domain from 109 ×129 to 93×113 grid cells (Fig.1). We extracted the last 3 years (2004-2006) of output to evaluate model performance over the entire U.S. relative to ground-based and satellite observations and standard WRF.

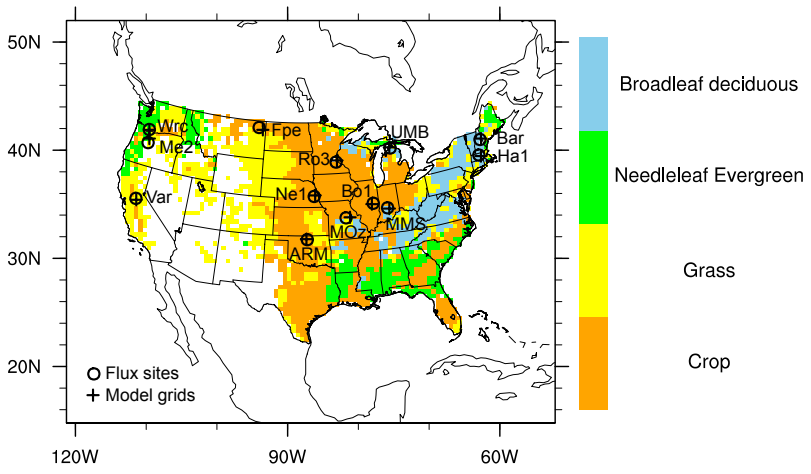

Figure 1 Distribution of the four dominant vegetation types in the model domain. The black circles indicate the AmeriFlux sites used in this work and plus signs are grid cells nearest to each observation site.

As part of the FLUXNET network, AmeriFlux is currently composed of 133 sites (both active and inactive) across North America, Central America and South America. The network collects continuous observations of ecosystem level exchanges of CO_2, water, energy, and momentum spanning diurnal, synoptic, seasonal, and interannual time scales. Thirteen AmeriFlux sites were used in the analysis. For most comparisons, we used the gap-filled Level 4 database, which has the best quality sensible heat flux (H) and latent heat flux (LE) data. Since lack of energy closure [*Wilson et al.*, 2002a] will affect the magnitude of observed H, LE, and G, we emphasize the Bowen Ratio comparison. Besides the gap-filled Level 4 data, we used Level 2 data with gaps for ground heat flux (G) (only for sites that had > 90% data), net radiation, and radiative fluxes (downward/upward solar and longwave radiation). In addition to the observed energy variables, we examined the three components of modeled latent heat flux: soil evaporation (LESOI), wet leaf evaporation (LEVEG), and dry leaf transpiration (LETRAN) to diagnose the model deficiencies even though there are no observations of these variables in the flux tower sites.

Although there are a total of 32 sites with Level 4 data from 2004 to 2006, we only used 13 sites (circles in Fig.1) in the analysis after a vegetation type match procedure. Because 50 km resolution and 4 or fewer PFTs per model grid cell are not directly comparable to site-level vegetation types, we assigned all model grid cells to one of four dominant vegetation types (cropland, grassland, evergreen needleleaf forest and deciduous broadleaf forest) according to the plant functional type with the highest percent (and a minimum of 30%) in the grid cell (Fig. 1). Even though broadleaf deciduous trees are not >50% of all BDT grid cells, PFT level fluxes and grid level energy fluxes are very well-matched from September to April, and grid level fluxes are only slightly less (<14 W m^{-2}) than BDT PFT level fluxes in summer. Then for each AmeriFlux site, we selected the nearest model grid cell with the same dominant vegetation type that occurs in the sites (Table 1). Nearest grid cells that were far away (>100km) from observation sites were not used.

We interpolated (using the inverse distance weighting method) the Clouds and the Earth's Radiant Energy System (CERES) Monthly TOA/Surface mean (SRBAVG) datasets [*Wielicki et al.*, 1996; *Young et al.*, 1998] into our model domain for a continental view of downward solar radiation, upward longwave radiation, and net radiation. CERES is a global satellite product that provides radiation fluxes at top-of-atmosphere and also at the surface (data are available for download at http://eosweb.larc.nasa.gov/PRODOCS/ceres/level3_srbavg_table.html).

We also used Parameter-elevation Regressions on Independent Slopes Model (PRISM) data [*Di Luzio et al.*, 2008] to evaluate the surface climatology (daily minimum temperature, daily maximum temperature, and precipitation). PRISM is recognized as one of the highest-quality spatial climate datasets over the United States. It synthesizes and interpolates point measurements of precipitation, temperature, and other climatic factors to produce continuous, digital grid estimates of monthly, yearly, and event-based climatic parameters with a 0.05 deg resolution (http://www.prism.oregonstate.edu/). As

with CERES, we interpolated the PRISM data to the model domain for the comparison with model output.

Table 1. Vegetation composition at AmeriFlux sites and corresponding model plant function types and percentages.

Site	Site Vegetation	Model PFTs							
		PFT 1	%	PFT 2	%	PFT 3	%	PFT 4 /other	%
				Cropland					
ARM	Wheat, corn, soybean periodic rotation	Crop	92	BDT Temperate	4	C3 grass	1	Bare Ground	3
Bo1	Corn, soybean annual rotation	Crop	93	BDT Temperate	7	-	-	-	-
Ne1	Maize	Crop	87	C3 grass	7	BDT Temperate	3	Bare Ground	3
Ro3	Corn, soybean annual rotation	Crop	72	C3 grass	16	BDT Temperate	10	Bare Ground	2
				Grassland					
Fpe	Grassland	C3 grass	65	Crop	14	BDT Temperate	2	Bare Ground	19
Var	Grazed C3 grassland in a region of savanna	C3 grass	76	NET Temperate	16	BDT Temperate	7	Bare Ground	1
				Evergreen needleleaf forest					
Wrc	Douglas-fir and western hemlock	NET Temperate	49	C3 grass	36	NET Boreal	12	BDT Temperate	3
Me2	Mature ponderosa pine	NET Temperate	53	C3 grass	33	NET Boreal	8	BDT Temperate	6
				Deciduous broadleaf forest					
MOz	Oak hickory forest	BDT Temperate	35	Crop	31	C3 grass	25	C4 grass	9
MMS	Mixed hardwood deciduous forest	BDT Temperate	54	C3 grass	24	Crop	20	C4 grass	2
UMB	Deciduous Broadleaf Forest	BDT Temperate	35	C3 grass	28	NET Temperate	20	Crop	17
Bar	Temperate northern hardwood forest	BDT Boreal	39	NET Boreal	31	C3 arctic grass	29	Crop	1
Ha1	Temperate deciduous forest	BDT Temperate	45	C3 grass	39	NET Temperate	11	Crop	5

BDT Temperate: Broadleaf deciduous tree- temperate, BDT Boreal: Broadleaf deciduous tree- boreal, NET Temperate: Needleleaf evergreen tree- temperate, NET Boreal: Needleleaf evergreen tree- boreal
ARM=ARM SGP Main, Bo1=Bondville, Ne1=Mead Irrigated, Ro3=Rosemount G19
Fpe=Fort Peck, Var=Vaira Ranch, Wrc=Wind river crane site, Me2=Metolius Intermediate Pine, MOz=Missouri Ozark, MMS=Morgan Monroe State Forest, UMB=UMBS, Bar=Barlett Experimental Forest, Ha1=Harvard Forest

Results

Surface climate

We compared the three-year (2004-2006) 2-meter daily mean minimum temperature (T_min), daily mean maximum temperature (T_max) and daily mean precipitation to PRISM data. The simulation has a warm bias with regional variation in magnitude. WRF3-CLM3.5 overestimated the T_min (Fig. 2a) over all of the United States, especially in the Midwest (> 8K), where most area is covered by crops or grassland. WRF3-CLM3.5's performance is better for T_max (Fig. 2b), with most of the West having a smaller warm bias (<4K) and some mountain areas underestimating the T_max by 4-6K. For all seasons, the Midwest has a consistent warm bias and the highest warm bias appeared in summer (not shown). Warm biases in the Midwest have also been seen in other combinations of climate and land surface models, such as RegCM-BATS [*Walker and Diffenbaugh*, 2009] and RegCM-CLM [*Tawfik and Steiner*, 2011] . WRF3-CLM3.5 underestimated precipitation (Fig.2c) in the Midwest, with some overlap between areas with a dry bias and the warm bias region. Low precipitation may be exacerbating the warmer climate in the overlap region. On the west and east coast, where there is forest cover, the model generally simulated more precipitation than in the PRISM dataset.

For the domain mean time series (Fig. 2d), the summer has the highest T_max difference, while the T_min bias is consistently large in all seasons (Fig. 2d). The large temperature bias also exists in standard WRF, with reduced summer T_max bias but increased winter T_min bias. Unlike the consistent year-to-year temperature bias, the precipitation bias has more interannual variation. For instance, summer has a large dry bias in 2004 and 2005, but not in 2006 (Fig. 2d). Compared to WRF3-CLM3.5, standard WRF shows a greater daily precipitation in nearly all months (Fig. 2d).

At the site-scale, WRF3-CLM3.5 has a consistent, large warm bias at the 13 flux tower sites in all seasons, with a range from +2.9K to +7.3K in the monthly mean bias (Table 2) averaged over each vegetation type. Cropland has the highest daily average 2 m temperature (T2) bias while evergreen forest has the lowest T2 bias. The daily precipitation bias has more seasonal variation among vegetation types. Generally WRF3-CLM3.5 overestimates the precipitation in winter and underestimates the precipitation in summer (not shown) at the 13 flux tower sites. With respect to monthly mean precipitation, the model simulated too little precipitation for crop and deciduous forest and excess precipitation for grasslands and evergreen forest (Table 2).

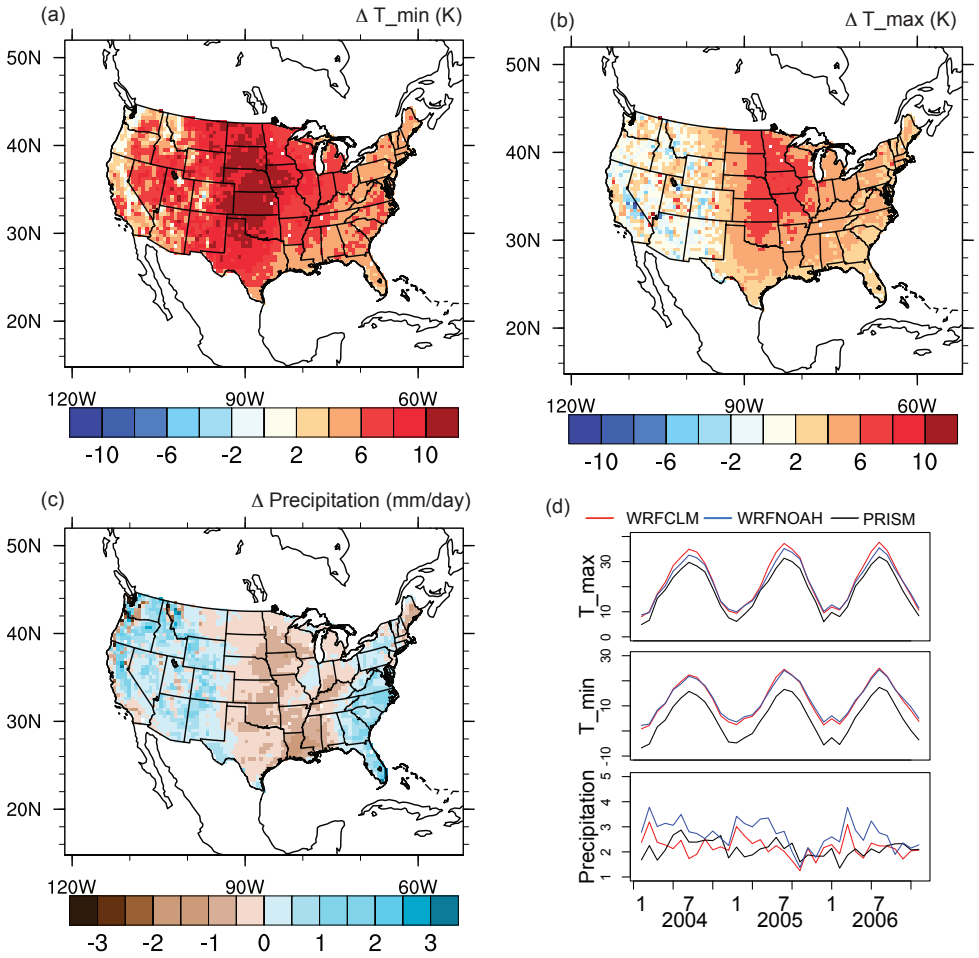

Figure 2. Annual difference in (a) minimum daily temperature, (b) maximum daily temperature, (c) daily precipitation between WRF3-CLM3.5 and PRISM from 2004 to 2006, and (d) monthly time series of T_max, T_min and precipitation averaged over the contiguous United States for WRF3-CLM3.5, standard WRF (WRFNOAH), and PRISM.

Table 2. Comparison of annual, site-level 2m temperature and daily precipitation between WRF3-CLM3.5 (model) and AmeriFlux (obs) averaged for the four vegetation types. Standard errors of the mean are given in parentheses, n indicates the number of sites for each vegetation type.

	n	2m temperature (°C)		Daily precipitation (mm/day)	
		model	*obs*	*model*	*obs*
Crop	4	19.1 (0.7)	11.8 (0.6)	1.8 (0.4)	2.2 (0.4)
Grass	2	16.2 (0.9)	10.6 (0.8)	2.0 (0.7)	1.4 (0.5)
Evergreen	2	11.5 (0.4)	8.6 (0.5)	5.5 (1.0)	3.6 (1.3)
Deciduous	5	13.7 (0.5)	9.9 (0.5)	2.7 (0.4)	2.8 (0.4)

Daily mean surface energy fluxes

The 13 observation sites we selected capture only a small subset of the area of each dominant vegetation type. Compared to hundreds of model grid cells, most of the observation sites are within the range of the WRF3-CLM3.5 simulation for latent heat flux (LE) (Fig. 3a). Modeled sensible heat flux (H) is generally greater than observed (Fig. 3b), consistent with WRF3-CLM3.5's warm bias. Flux values at the nearest grid cells tend to be higher than observations for both fluxes for all dominant vegetation types.

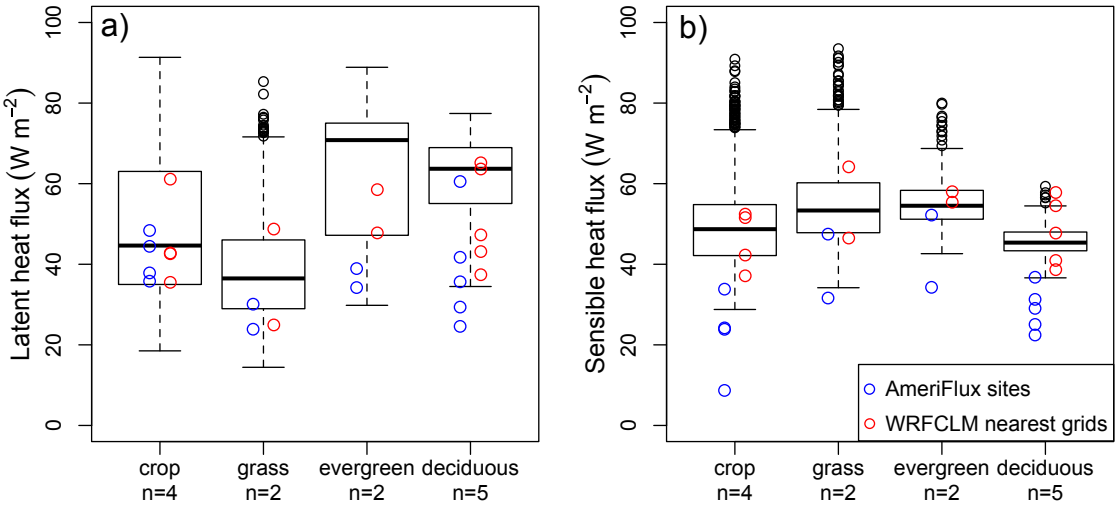

Figure 3. Three years (2004-2006) of daily mean (a) latent heat flux and (b) sensible heat flux for the four dominant vegetation types evaluated. The bottom and top of each box are the 25th and 75th percentile (the lower and upper quartiles, respectively) among all grid cells for the dominant type, and the band near the middle of the box is the 50th percentile. The ends of the whiskers are the lowest and highest data points still within 1.5 times the interquartile range. Black circles are outliers, blue circles are the three-year daily mean fluxes over 13 AmeriFlux towers (black circles in Fig. 1), and red circles are mean fluxes for the grid cells nearest to observation sites (plus signs in Fig.1); "n" indicates the number of observed sites for each vegetation type.

Monthly variation in surface energy partitioning

WRF3-CLM3.5's performance for monthly partitioning of surface energy is shown for 8 out of the 13 sites in Fig. 4, with two representative sites for each vegetation type. Ground heat flux (G) was only available at four sites (Na1, Var, Me2 and MMS) where percent of data available is greater than 90%. Without an irrigation scheme in the model, WRF3-CLM3.5 produced lower LE at irrigated crop sites Ne1 while partitioning more energy to H in the summer (Fig. 4a). Irrigation at Ne1 results in an observed increase in LE in summer (maximum in August, 114.9 W m^{-2}) corresponding with a decrease in H (minimum in August, 7.8 W m^{-2}). However, WRF3-CLM3.5 produced a large H (85.7 W m^{-2} in August) and small LE (41.2 W m^{-2} in August) in summer. Similar patterns were found at two non-irrigated sites (Ro3 and Bo1) could due to the underestimated precipitation or leaf area index. At the non-irrigated ARM site, the model reasonably

simulated monthly variation in H and LE with a slightly higher magnitude than observed (annual average of 17.8 W m^{-2} greater H and 6.9 W m^{-2} greater LE).

Due to different climate conditions, observed energy fluxes indicate a clear difference in the timing of the growing season at the two grass sites (Fig 4b), which is not replicated by the model. The growing season is spring and summer at Fpe, which has a continental climate, but is winter and spring at Var due to the Mediterranean climate. The growing season usually is associated with large LE due to greater soil evaporation and plant transpiration. The flux tower measurements do show a maximum LE in July at Fpe (86.6 W m^{-2}) and in April at Var (63.1 W m^{-2}). However, simulated H and LE at Fpe and Var have a very similar temporal pattern (gradually increasing in spring, reaching peak in summer). Such a pattern is reasonable at Fpe but is incorrect at Var where the natural grass has senesced in summer.

For the evergreen forest sites, the energy flux simulations have a pattern similar to the observations, but with greater magnitude (Fig.4c). The annual averaged LE and H differences are 13.6 W m^{-2} and 4.8 W m^{-2} greater than observed at the Wrc site and 21 W m^{-2} and 19.6 W m-^{2} greater at the Me2 site.

For the deciduous forest sites (Fig.4d), the flux observations indicated the clear growing season pattern of deciduous broadleaf trees, which was not represented in the simulations. All AmeriFlux deciduous sites observed an LE increase in spring and summer accompanied by a decrease in summer H when new leaf growth generates stronger photosynthesis and enables more transpiration at the surface. In the simulation, H peaks in the summer season, which is not in agreement with the observation of a peak in March and April before leaf emergence. The same results were observed at the UMBS site for a different time period [*Schmid et al.*, 2003]. At MMS and Ha1, H was correctly simulated before May, but continued to increase and reached peaks in June (Ha1) and August (MMS), while observed H decreased after April. LE was overestimated at Ha1 in most of the months by an average of 18.5 W m^{-2} and MMS was overestimated in spring and winter by an average 17.9 W m^{-2}.

In the model, G is calculated as net radiation (Rn) minus H and LE, therefore errors in Rn, H, and LE could all contribute to the G bias making it hard to diagnose. The simulated G is higher than observations in nearly all months, and the bias magnitude ranges from 1 W m^{-2} to 4 W m^{-2} over the four sites with adequate data (Ne1, Var, Me2, and MMS, right panels in Fig. 4).

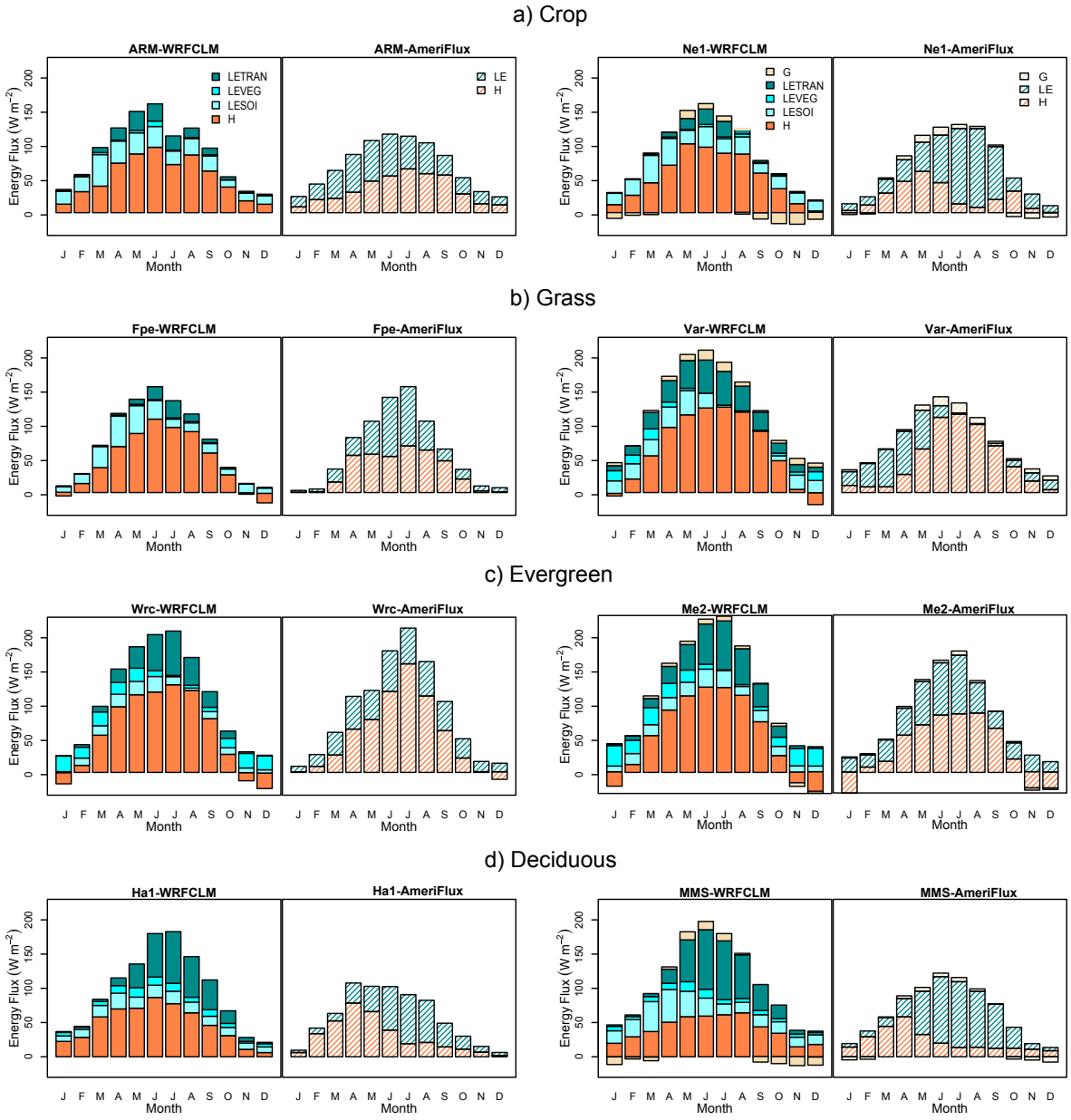

Figure 4. Seasonal energy partitioning (2004-2006 mean) for four dominant vegetation types at 8 observation sites (hashed bars) and the nearest grid cells (solid bars). H is sensible heat flux, LE is latent heat flux, LESOI is soil evaporation, LEVEG is leaf evaporation, LETRAN is leaf transpiration, and G is ground heat flux. Observed H and LE are Level 4 Ameriflux data. G is Level 2 data and only available for select sites.

The Bowen ratio comparison shown in Figure 5 indicates that the model is good at capturing the monthly partitioning for evergreen forest vegetation, but misses features of the monthly patterns for cropland, grassland, and deciduous forest. For cropland, both WRF3-CLM3.5 and standard WRF overestimated the Bowen ratio (1.3-1.8) due to underestimated latent heat flux. The observed crop Bowen ratio (Fig. 5a) was very low (0.26-0.36) between May and September due to increased latent heat flux introduced by

irrigation or rainfall. Over the four crop sites, the Bowen ratio from April to September (growing season) was 1.25 for ARM site, 0.75 for Ne1, 0.58 for Bo1, and 0.42 for Ro3. For grassland (Fig. 5b), instead of showing the average of the two sites, we plot the Bowen ratios individually since the two sites have very different climates. At the Var site, the observed Bowen ratio is very large (9-21, peak in September) due to little LE and very large H. WRF3-CLM3.5 did not capture the peak while standard WRF overestimates the peak by 13. The large standard errors in the observed summer Bowen ratio realistically reflect the large variation in observed H and LE at the Var site, which suggests challenges for accurate simulations over grassland areas. The underestimated Bowen ratio by WRF3-CLM3.5 in summer is mainly due to excess LE at the Var site. The source of the incorrect LE can be explained by excess plant transpiration (Fig. 4b) due to a too large leaf area index in summer. At the Fpe site, both WRF3-CLM3.5 and standard WRF slightly overestimate the Bowen ratio. For evergreen forest (Fig. 5c), although the magnitude of the simulated H and LE are both higher than observed (Fig. 3), the Bowen ratio matches observations quite well. Notably, the WRF3-CLM3.5 simulation of energy partitioning performs better than standard WRF for evergreen forests in most months. For deciduous forest (Fig. 5d), the simulated Bowen ratio is much smaller than observed in spring due to excessive LE (H values are reasonable). Similar to evergreen forest, standard WRF simulated a lower Bowen ratio compared to WRF3-CLM3.5.

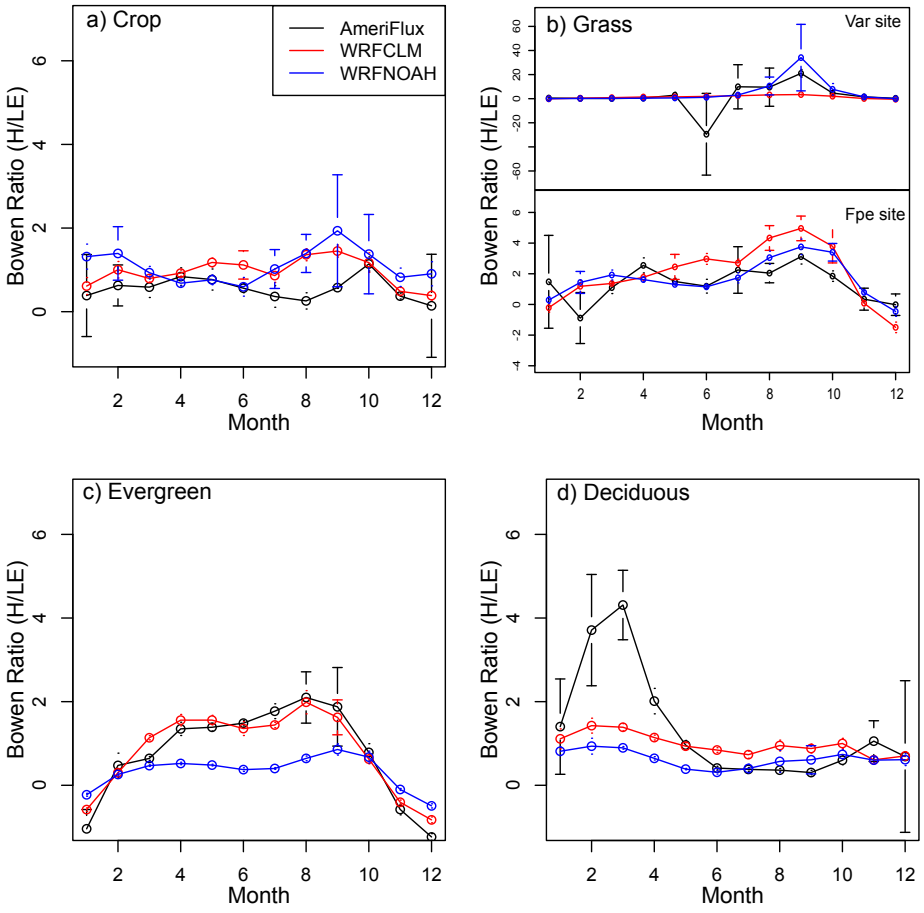

Figure 5. Monthly Bowen Ratio for a) cropland, b) grassland, c) evergreen needleleaf forest, and d) broadleaf deciduous forest comparing WRF3-CLM3.5 (WRFCLM), standard WRF (WRFNOAH), and Ameriflux observations. The WRFCLM and WRFNOAH values are the mean of nearest grid cells for each type (plus signs in Fig. 1), and the observation values are the mean of the Ameriflux sites (black circles in Fig. 1). The error bars indicate the standard errors (n = 3 years). For grassland, instead of showing the average of the two sites, we plot the Bowen ratios individually for Fpe and Far site since the two sites have very different climates.

Surface radiation budgets

The simulation of surface to atmosphere energy fluxes is highly dependent on the surface radiation budget. Net radiation is the balance between net solar radiation and net longwave radiation. Incorrect simulation of the radiation budget affects the magnitude of the components of the surface energy balance. And in the nonlinear climate system, the magnitude change for H, LE and G may not be the same; therefore the bias in the radiation budget could alter surface energy partitioning.

The relatively reasonable simulation of continental-scale net radiation (Fig. 6a) is due to two canceling errors. Over-predicted upward longwave radiation (Fig. 6b) is canceled by the over-predicted downward solar radiation (Fig. 6c). For most regions, the bias in mean net radiation is not large (within ±15 W m^{-2}) compared to the bias in downward solar radiation (40-60 W m^{-2}) and upward longwave radiation (20-60 W m^{-2}). In the Midwest, where the warm bias is quite large, the bias in net radiation is actually low (20 W m^{-2}). This is because the higher surface temperature in this region generates higher upward longwave radiation, by 70 W m^{-2}.

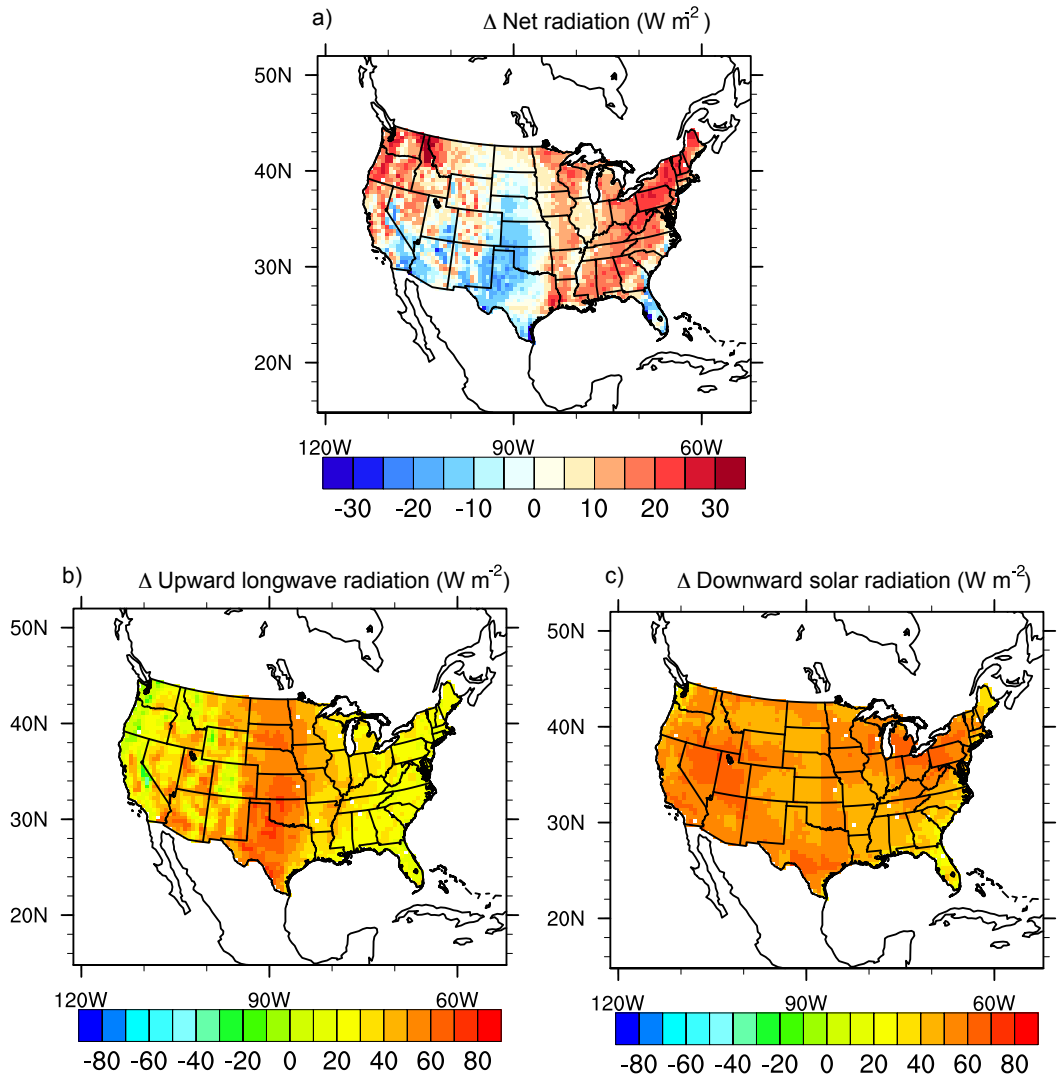

Figure 6. Annual differences between WRF3-CLM3.5 and CERES in 2004 for (a) net radiation, (b) upward longwave radiation, and (c) downward solar radiation.

At the site level, the model generated 20% or more excess net solar radiation and longwave radiation for all four vegetation types (Table 3), further confirming a systematic over-estimation. The excess downward solar radiation for all vegetation types is a discrepancy that has been found in many climate models [*Wild*, 2008]. We also found that WRF3-CLM3.5 tends to produce a larger downward solar radiation bias in summer than in winter (not shown), which may be due to 20% less cloud cover in summer but not winter (using a rough comparison to CERES cloud cover data, not shown). As would be expected, the model produces excess upward (emitted) longwave radiation due to the overestimated surface temperature. The large bias also dominates the net longwave flux since the bias in downward longwave is negligible except for over crops (Table 3). The temporal variation in the net radiation bias is similar to the downward solar radiation bias: higher in summer than winter (Fig 7), which highlights that downward solar radiation is fundamentally important to correct simulation of net radiation.

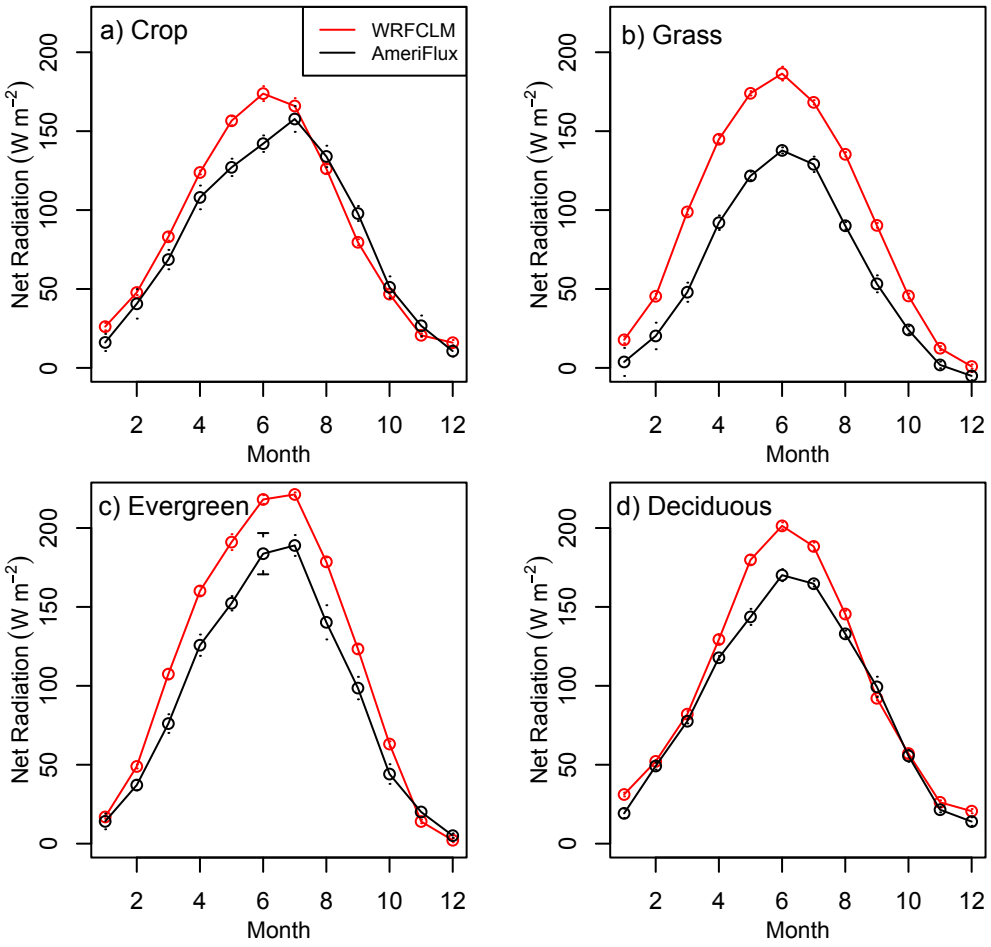

Figure 7. Monthly net radiation for WRF3-CLM3.5 nearest grid cells (red line) and Ameriflux sites (black line) for a) cropland, b) grassland, c) evergreen needleleaf forest, and d) broadleaf deciduous forest in 2004.

Table 3. Surface radiation budgets of WRF3-CLM3.5 (model) (obs) over four dominant vegetation types. Values for cropland (crop), grassland (grass), evergreen needleleaf forest (evergreen) and deciduous broadleaf forest (deciduous) are the averages over sites for each dominant vegetation type (Table 1).

	Net radiation		SW down		SW up		Net SW		LW down		LW up		Net LW	
	Model	*Obs*	*Model*	*Obs*	*Model*	*Obs*	*Model*	*Obs*	*Model*	*Obs*	*Model*	*Obs*	*Model*	*obs*
Crop	88.9	81.7	221.9	191.9	35.2	40.2	186.7	151.7	332.6	371.5	430.4	379.8	-97.8	-8.3
Grass	93.3	59.7	231	183.5	39.2	43.8	191.8	139.7	307.4	302.5	405.9	376.5	-98.5	-74
Evergreen	112.1	90.5	203.6	165.8	23.9	17.8	179.7	148	308.3	304.2	375.9	360.3	-67.6	-56.1
Deciduous	100.5	88.8	209.9	164.6	29.7	23.8	180.2	140.8	320.9	317.8	400.6	371.1	-79.7	-53.3

SW down: downward solar radiation, SW up: upward solar radiation, Net SW: net solar radiation, LW down: downward longwave radiation, LW up: upward longwave radiation, Net LW: net longwave radiation.

Discussion

Both WRF and CLM have deficiencies that should be resolved in future versions to reduce the warm bias. The large warm bias in the standard version of WRF suggests there are problems in WRF. For example, the downward solar radiation bias contributes substantially to the warm bias based on a one-year sensitivity test that artificially reduced downward solar radiation by 30% (WRF3-CLM3.5 simulated a 3K lower 2 meter air temperature averaged over land grid cells). Reducing downward solar radiation is not simple because it is associated with many factors. Previous work [*Markovic et al.*, 2008; *Wild et al.*, 2001] suggests the overestimate of downward solar radiation at the surface could be either due to less cloud cover for cloudy days or less sky absorption of downward solar radiation for clear days. Ignoring aerosols in the model may also contribute to excess downward solar radiation [*Wild*, 2008]. The negative precipitation bias in the Midwest (Fig. 2c) suggests that an underestimate of cloud cover may contribute to excess downward solar radiation in the Midwest. Further validation with WRF3-CLM3.5 focusing on the cloud cover and clear sky absorption are strongly encouraged but are beyond the scope of this paper.

Fortunately, the newer WRF3.2 includes boundary layer physics and microphysics that could improve the overall simulation. A one-year sensitivity test using standard WRF3.2 with the MYNN boundary scheme [*Nakanishi and Niino*, 2009] and Thompson microphysics scheme [*Thompson et al.*, 2008] showed a reduction in the downward solar radiation by 30 W m^{-2}, in T_max by 3K, and in T_min by 2K.

With respect to CLM, the large warm bias in the Midwest could be due in part to 1) the missing irrigation scheme, and 2) the lower crop leaf area index used in the model. A large area in the Midwest is covered by irrigated agriculture according to global irrigation maps [*Siebert et al.*, 2005]. Without an irrigation scheme, WRF3-CLM3.5 may overestimate temperature by 3-5K in summer in the Midwest [*Lobell et al.*, 2009; *Sacks et al.*, 2009]. Considering the strong coupling between soil moisture and precipitation in the Midwest [*Koster et al.*, 2004], low soil moisture could reduce cloud cover and enhance the downward solar radiation, further heating the land surface and contributing to a positive feedback in this region and producing a large warm bias. Also, the much lower maximum leaf area index used in the model (Table 4) could reduce LE and therefore increase H and near-surface temperature. The simulated seasonal variation in LAI is much lower than the direct measurements at the Bo1 site [*Wilson and Meyers*, 2007].

Table 4. Comparison of maximum leaf area index between model and observation for Ameriflux sites with measurements (obs) and corresponding model grid cells (model).

	Max Leaf area index	
	Model	*Obs*
Crop[1]	1.91	6.6
Grass[2]	1.4	2.45
Evergreen[3]	4.3	3.62
Deciduous[4]	4.2	4.5

[1]Crop: the mean maximum leaf area index at Bon, Ne1 and Ro3.
[2]Grass: the mean maximum leaf area index at Fpe and Var.
[3]Evergreen: the mean maximum leaf area index at Wrc and me2.
[4]Decidous: the mean maximum leaf area index at MOz, MMS, UMB, Bar and Ha1.

Although CLM3.5 includes significant improvements in surface input data [*Lawrence and Chase*, 2007], there is still space for further improvements due to uncertainties in algorithm and validation methods used to produce the surface data [*Yang et al.*, 2006]. In particular, leaf area index (LAI) is a key physiology parameter that strongly influences the LE and surface albedo. With lower LAI, the model may generate lower LE if other conditions remain the same. The lower LE would shift the Bowen ratio, increasing the near surface temperature and even possibly reducing precipitation due to less water vapor transport. For example, the underestimated LE at the Fpe site may be because of the lower LAI used in the model, which is 1.4 m^2 m^{-2} for maximum LAI while the observed LAI is 2.5 m^2 m^{-2} (Table 4). The mean maximum LAI over the crop sites is 6.6 m^2 m^{-2}, while the model mean maximum value is 1.9 m^2 m^{-2}, which reduced the partitioning to LE in WRF3-CLM3.5. Although the prescribed LAI in the model does not capture the observed interannual variability [*Lu et al.*, 2001], LAI in WRF3-CLM3.5 is quite good for three deciduous sites (Fig. 8), where the observed LAI values are similar to the model values. At Ha1, the observed LAI is larger than the model LAI, but the lower LAI in the model yielded a larger LE, which suggests that there are other factors driving the overestimated LE. For instance, the large LE and H in summer may be due to the excess net radiation (Figure 7). Overestimated precipitation in February and March may also help account for the high LE in those months.

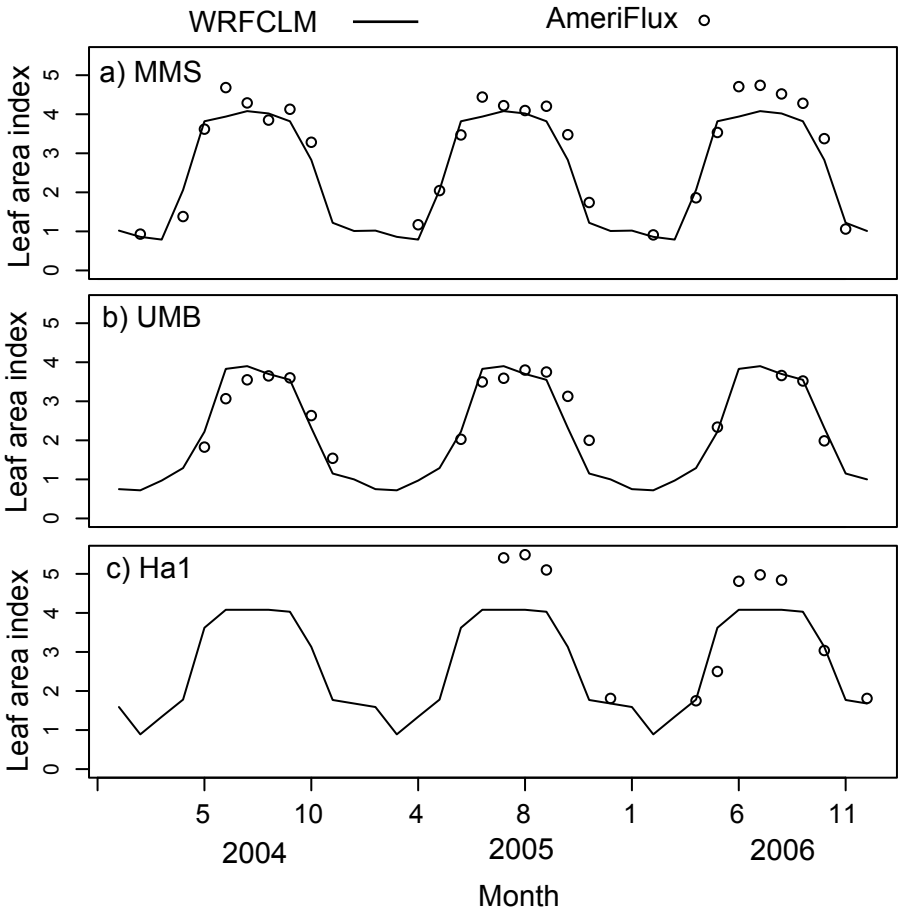

Figure 8. Monthly variation in leaf area index for WRF3-CLM3.5 and AmeriFlux observations at three deciduous sites, (a) MMS, (b) UMB and (c) Ha1. LAI used in WRF3-CLM3.5 is an interpolation of CLM3.5 standard input [*Lawrence and Chase*, 2007], a prescribed LAI that does not change from year to year (lines). The LAI at AmeriFlux sites are ground observations available for some months (circles).

In CLM3.5, an additional soil resistance term [Sellers et al., 1992] was added that effectively reduced the unreasonably large soil evaporation in CLM3 [Lawrence et al., 2007]. However, our simulation (Fig. 4d) suggests that the excessive soil evaporation is still a problem for broadleaf deciduous forest before leaf emergence in January, February, and March, which is also supported by offline simulations [Stockli et al., 2008]. At Ha1 and MMS (Fig. 4d), it is obvious that the soil evaporation (LESOI) is the largest among the three LE components in spring. The large soil evaporation substantially reduced the Bowen ratio before leaf emergence. The new treatment of soil evaporation in the latest version of CLM [*Sakaguchi and Zeng*, 2009] reduced the annual average soil evaporation, but mostly in summer in the U.S. [*Lawrence et al.*, 2011]. Further improvements to reduce spring soil evaporation in broadleaf deciduous regions are highly recommended.

Conclusion

Our analyses show that WRF3-CLM3.5 output is in good agreement with observed energy partitioning over needleleaf evergreen forests, but has errors in cropland, grassland and broadleaf deciduous forest. Since none of the current climate models can perfectly simulate energy fluxes and standard WRF has a large wet bias, we believe WRF3-CLM3.5 could be usefully applied in land use conversion research after specific improvements. One recommendation that could immediately improve the simulation is correcting LAI based on available ground observations. For studies focused on the Midwest U.S., irrigation processes must be added as in [*Sacks et al.*, 2009] for a better simulation not only of energy fluxes, but also of temperature and precipitation, due to the strong soil moisture-precipitation feedback. After adding irrigation processes and correcting the LAI, WRF3-CLM3.5 should be reliable for studying conversions between grassland, dryland crops and irrigated crops, or between needleleaf evergreen forest and grassland. Studies involving deciduous forests need to consider the excessive spring soil evaporation that cannot be easily corrected in the current model version.

Our analysis shows that a large warm bias exists both in standard WRF and WRF3-CLM3.5, and that this bias is substantially diminished when downward solar radiation is artificially reduced, suggesting that the WRF model has some deficiencies independent of the land surface model. The very large downward solar radiation in WRF is the driving force for the warm bias, which could be due to too little cloud cover or insufficient sky absorption of downward solar radiation on clear days. Further examination of these potential deficiencies are beyond the scope of this paper, but will be important for improving the quality of regional climate model studies using WRF. A more recent version of WRF includes new schemes for microphysics and boundary layer physics [*Nakanishi and Niino*, 2009; *Thompson et al.*, 2008] that also may improve the overall simulation.

CHAPTER 2

Evaluation of a regional coupled climate-cropland model (WRF3.3-CLM4crop) with irrigation practice

Introduction

The response of agricultural systems to changing climate has attracted considerable attention due to increased potential for global food crises [*Adams et al.*, 1990; *Lawlor and Mitchell*, 1991; *Long et al.*, 2006; *Mendelsohn et al.*, 1994; *Rosenzweig and Parry*, 1994]. Crop models, including phenology process based model and statistical models, are widely used to simulate climate impacts on crop growth and production. For example, warming by 2-4 ^{o}C could shorten the growing season and alter crop calendars [*Butterfield and Morison*, 1992; *Peiris et al.*, 1995], elevated CO2 can increase crop yield [*Brown and Rosenberg*, 1999; *Easterling et al.*, 1992; *Mearns et al.*, 1992], and crop regression models suggest that yields of wheat, maize, and barley are declining with increased temperature globally [*Lobell and Field*, 2007; *Lobell et al.*, 2008b]. Although agronomic models have increased our understanding of crop responses to climate change, they have not accounted for interactions between climate and crop growth.

Crop growth and climate are highly coupled. Optimum soil temperature and moisture yield the maximum seed germination rate for a given crop [*Covell et al.*, 1986; *Wagenvoort and Bierhuizen*, 1977]. Growing degree days (sum of daily degrees above a baseline) based on the air temperature determines the phenological phase and physiological activity of crops [*Bonhomme*, 2000]. Furthermore, crop productivity is reduced by many forms of environmental stress, such as extreme temperature, drought, and air pollution [*Pessarakli*, 1999]. At the same time, cropland plays a very important biogeophysical role in changing climate [*Feddema et al.*, 2005; *Foley et al.*, 2005; *Pitman et al.*, 1999]. Crops alter the small-scale boundary layer structure [*Adegoke et al.*, 2007], such as surface wind and boundary layer height, by increasing canopy height during the growth process. Compared to natural vegetation, cropland has higher albedo that alters the energy budget when converting between forest and cropland [*Bonan*, 2008; *Oleson et al.*, 2004]. Cropland also alters the water cycle. Both field observations and modeling have shown that conversion of forest to cropland can reduce evaportranspiration and precipitation at the regional scale [*Sampaio et al.*, 2007].

Cropland management, such as irrigation, has been found to alter climate at global and regional scales [*Adegoke et al.*, 2003; *Cook et al.*, 2011; *Harding and Snyder*, 2012; *Jin and Miller*, 2011; *Ozdogan and Salvucci*, 2004; *Sorooshian et al.*, 2011]. The extra water applied to the soil enhances evapotranspiration, thereby reducing surface temperature through evaporative cooling [*Kueppers et al.*, 2007b; *Lobell et al.*, 2009; *Sacks et al.*, 2009]. Condensation of the water vapor in the atmosphere releases latent heat that provides energy for cloud convection and precipitation [*DeAngelis et al.*, 2010; *Saeed et al.*, 2009], an effect that can propagate to neighboring regions [*Lo and Famiglietti*, 2013].

The surface cooling reduces emission of surface long wave radiation, while the water vapor in the upper air can absorb and release more long wave radiation to the surface [*Boucher et al.*, 2004; *Kueppers and Snyder*, 2012], thereby increasing the surface net radiation. Irrigation also can increase net solar radiation at the surface due to the decreased albedo of wet soil [*Otterman*, 1977]. A key issue is that the simulation models used to explore these mechanisms have prescribed crop leaf area values that do not respond to environmental change or inter-annual variation in weather and climate. This prescribed approach could overestimate and underestimate evapotranspiration from croplands, depending on time of year and environmental conditions, because crop leaf area and physiological activity are known to dynamically respond to climate variation [*Fang et al.*, 2001; *Porter and Semenov*, 2005].

Coupling of process-based crop growth models into climate model enables simulation of the two-way interactions between climate and crop growth. Recent work incorporating crop growth models into climate models has revealed that dynamic crop growth strongly influences regional climate patterns by altering land surface water and energy exchange [*Bondeau et al.*, 2007b; *Levis et al.*, 2012; *Liang et al.*, 2012; *Lu et al.*, 2001; *Osborne et al.*, 2007; *Tsvetsinskaya et al.*, 2000; *Xu et al.*, 2005]. Most of these studies have not rigorously evaluated results against observations of climate and crop variables. Further, interactions between crop growth and irrigation effects on climate are not well examined. Therefore, our objectives were to, 1) evaluate a newly coupled regional climate-cropland model's performance in simulating crop growth and surface climate using multiple observational datasets, and 2) investigate interactions between irrigation and dynamic crop growth effects on surface climate.

Methods

Regional climate model

We coupled the Community Land Model version 4 (CLM4) to the Weather Research and Forecasting Model version 3.3.1 (WRF3.3) to utilize an advanced land model for simulations of the effects of crop growth and irrigation on regional climate. CLM4 includes new treatments of soil column-groundwater interactions, soil evaporation, aerodynamic parameters for sparse/dense canopies, vertical burial of vegetation by snow, snow cover fraction and aging, black carbon and dust deposition, and vertical distribution of solar energy [*Lawrence et al.*, 2012; *Oleson et al.*, 2010]. The CLM land surface model improved minimum temperature and precipitation over the Noah land surface model in simulations using an earlier version of the coupled model (WRF3.0-CLM3.5) [*Jin et al.*, 2010; *Lu and Kueppers*, 2012; *Subin et al.*, 2011]. However, we also found that the CLM prescribed crop leaf area index in the Midwest was lower than observations, potentially contributing to a large warm bias [*Lu and Kueppers*, 2012]. Further, in both Noah and CLM4, as for natural vegetation, crop plant parameters, such as leaf area index and stem area index are fixed for each month and do not change from

year to year. This limits the usefulness of WRF3.0-CLM3.5 for studying two-way interactions between crops and climate.

To better simulate interactions between the atmosphere and cropland, we further developed a crop version of the coupled model (WRF3.3-CLM4crop) that simulates dynamic crop growth following work by Levis and colleagues [2012]. Crop growth has large inter-annual variability with a large impact on surface energy and water cycles [*Lu et al.*, 2001]. While it was ignored in early land surface models, recently, several land surface models have integrated dynamic crop growth, which has improved temperature and precipitation simulations relative to observations [*Bondeau et al.*, 2007b; *Gerten et al.*, 2004; *Krinner et al.*, 2005; *Levis et al.*, 2012; *Osborne et al.*, 2007; *Sitch et al.*, 2003; *Tsvetsinskaya et al.*, 2000]. The details of the WRF3.3-CLM4crop crop growth parameterization and modification are described in Appendix A, but are briefly summarized here. The new dynamic crop growth module updates the leaf area index (LAI); stem area index; canopy height; and leaf, stem, grain, and root carbon at each time step and the values vary from year to year, depending on environmental conditions. The LAI, stem area index, and canopy height are used in hydrology and radiation modules to calculate the energy and water state variables that are transferred into the atmospheric model. LAI and plant carbon allocation differ according to phenological stage (planting, leaf emergence, grain filling, and harvest). Transitions between phenological stages are controlled by growing degree days (with a base of 8 °C for C3 crops and 10 °C for C4 crops).

Irrigation scheme

We adopted a precision agriculture-type irrigation scheme, where the amount and timing of irrigation simulates efficient irrigation practices. Irrigation water is applied as a function of root water stress (β_t), leaf temperature (T_{veg}) and LAI. The root water stress is monitored by β_t, which varies from near zero (dry soil) to one (wet soil). Leaf temperature also is used not only to more realistically simulate irrigation systems [*Howell et al.*, 1984; *Wanjura et al.*, 1992], but also to maintain optimum plant growth because high leaf temperature can inhibit plant photosynthesis [*Wise et al.*, 2004]. Irrigation starts after leaf emergence (LAI>0.1 m^2 m^{-2}), and occurs when either plant water is low (β_t <0.99) or leaf temperature is too high (T_{veg} >35°C). Irrigation water is applied in the form of rain at a constant rate of 0.0002 mm s^{-1}, selected to match the range of current irrigation systems (4-20 gallons per minute per acre). Cropland equipped for irrigation (Figure 9a) was derived from the 0.05 deg global irrigation map [*Siebert et al.*, 2005], as updated in 2006 (http://www.geo.uni-frankfurt.de/ipg/ag/dl/forschung/Global_Irrigation_Map/index.html). The simulated annual irrigation water use (Figure 9b) is within 14% of U.S. water usage estimated by USGS for 2005 [*Kenny et al.*, 2005]. The range in annual simulated irrigation water use from 2004-2006 was 113-149 billion gallons per day (143 for 2005); the USGS survey estimates 128 billion gallons per day in 2005 (http://ga.water.usgs.gov/edu/wuir.html).

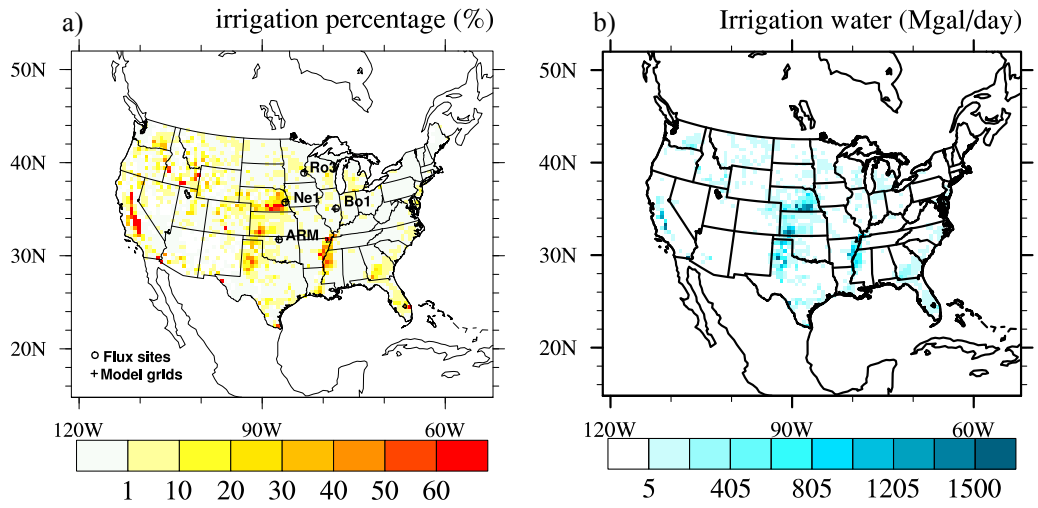

Figure 9. Modeled domain showing a) percent of cropland equipped for irrigation (%) within each grid cell (Siebert et al. 2005), and b) mean 2004-2006 irrigation water applied (million gallons per day) simulated in WRF3.3-CLM4crop. The four AmeriFlux observational sites are indicated in (a).

Experiments design

We set up two 10-year (2002-2011) simulations using WRF3.3-CLM4crop to evaluate crop growth (leaf area index and growing season length). One is a control simulation without irrigation (hereafter referred to as CROP), and the other includes irrigation (hereafter referred to as CROPIRR). In addition, we set up two additional 5-year (2002-2006) standard simulations with (hereafter referred to as STDIRR) and without irrigation (hereafter referred to as STD) using the prescribed LAI version of the coupled model (WRF3.3-CLM4) to quantify interactive effects of dynamic crop growth and irrigation on surface air temperature and energy fluxes. The physical modules used in all simulations include the MYNN boundary layer scheme [*Nakanishi and Niino*, 2006], the CAM longwave/shortwave radiation scheme [*Collins et al.*, 2004], the new Grell cumulus scheme [*Grell and Devenyi*, 2002], and the Thompson microphysics scheme [*Thompson et al.*, 2004]. The simulations focused on the continental United States (U.S.) with 25 vertical layers and 50 km horizontal resolution. We interpolated (using the inverse distance weighting method) 0.5 deg CLM surface input data (including plant functional types, plant function type percent, leaf area index, and stem area index) into the model domain. We used NCEP/DOE Reanalysis II data as lateral boundary conditions [*Kanamitsu et al.*, 2002]. For analysis, we removed 8 grid cells from the full perimeter of the domain as a buffer, which diminished the original domain from 109 ×129 to 93×113 grid cells. The first two years of the simulations were discarded as spin-up and the analysis focused on the final 8 years (2004-2011).

Validation data

We validated leaf area index (LAI), sensible heat flux (H), and latent heat flux (LE) at four AmeriFlux sites in the Midwest (showed on Figure 9a). We obtained 9-years (2002-2010) of LAI data [*Fischer*, 2005] at ARM SGP Main (SGP), which is measured with a light wand (Licor LAI-2000) during the active growing season (Marc Fischer, personal correspondence) from 2002 -present. We downloaded LAI measurements at three other sites (Bondville, Mead irrigated, Mead rainfed) from ftp://cdiac.ornl.gov/pub/ameriflux/data/Level2/AllSites/biological_data/. Model LAI (for crop PFTs only), H, and LE were extracted at the grid cell nearest to each site from the CROP simulation for non-irrigated sites (SGP, Bondville, Mead rainfed, Rosemount-G19) and from the CROPIRR simulation for Mead irrigated site. We compared monthly variation in LAI and interannual variation in peak LAI. For the monthly LAI comparison, the simulated LAI is the 10-year (2002-2011) averaged monthly LAI, while the observed LAI is averaged over different numbers of years depending on availability of observations. We didn't compare peak LAI variation at Bondville because observations were only available for 5 years, 1997-2001. For H and LE, we compared three year (2004-2006) averaged monthly variation using gap-filled level 2 observations.

We used in-situ soil moisture data from the international soil moisture network (http://www.ipf.tuwien.ac.at/insitu/). Over the validation period 2004-2006, the soil moisture measurements are available from SCAN, SNOTEL, ARM, and AmeriFlux networks. Sites measured the soil moisture at different depths, which differ from the soil depths used in WRF3.3-CLM4crop. Therefore, we compared the soil water (mm) in the upper soil (0-50 cm) instead of directly comparing the soil water content (m^3 m^{-3}) at each soil layer. After a data quality control procedure (missing values < 10%), we selected 18 SCAN sites, 47 SNOTEL sites, 10 ARM sites, and 9 AmeriFlux sites.

We validated the 3-year (2004-2006) daily mean temperature (an average of minimum and maximum temperature), dew point temperature and precipitation using the Parameter-elevation Regressions on Independent Slopes Model (PRISM) 4km product [*Di Luzio et al.*, 2008]. We interpolated the PRISM values to the model domain for comparison with model output.

Results

Model evaluation

1) Leaf area index (LAI) comparison

Compared to site observations, the dynamic crop growth model overestimated monthly LAI in most months and sites, displayed a longer growing season, and failed to capture the rapid decline of LAI after the peak (Figure 10). The prescribed LAI and MODIS LAI both underestimated the site-based LAI and showed no difference at the Mead irrigated and rainfed sites. While the dynamic crop growth model correctly increased LAI at Mead with the added irrigation scheme, the magnitude of the LAI difference is much larger than the observed difference between Mead irrigated and Mead rainfed.

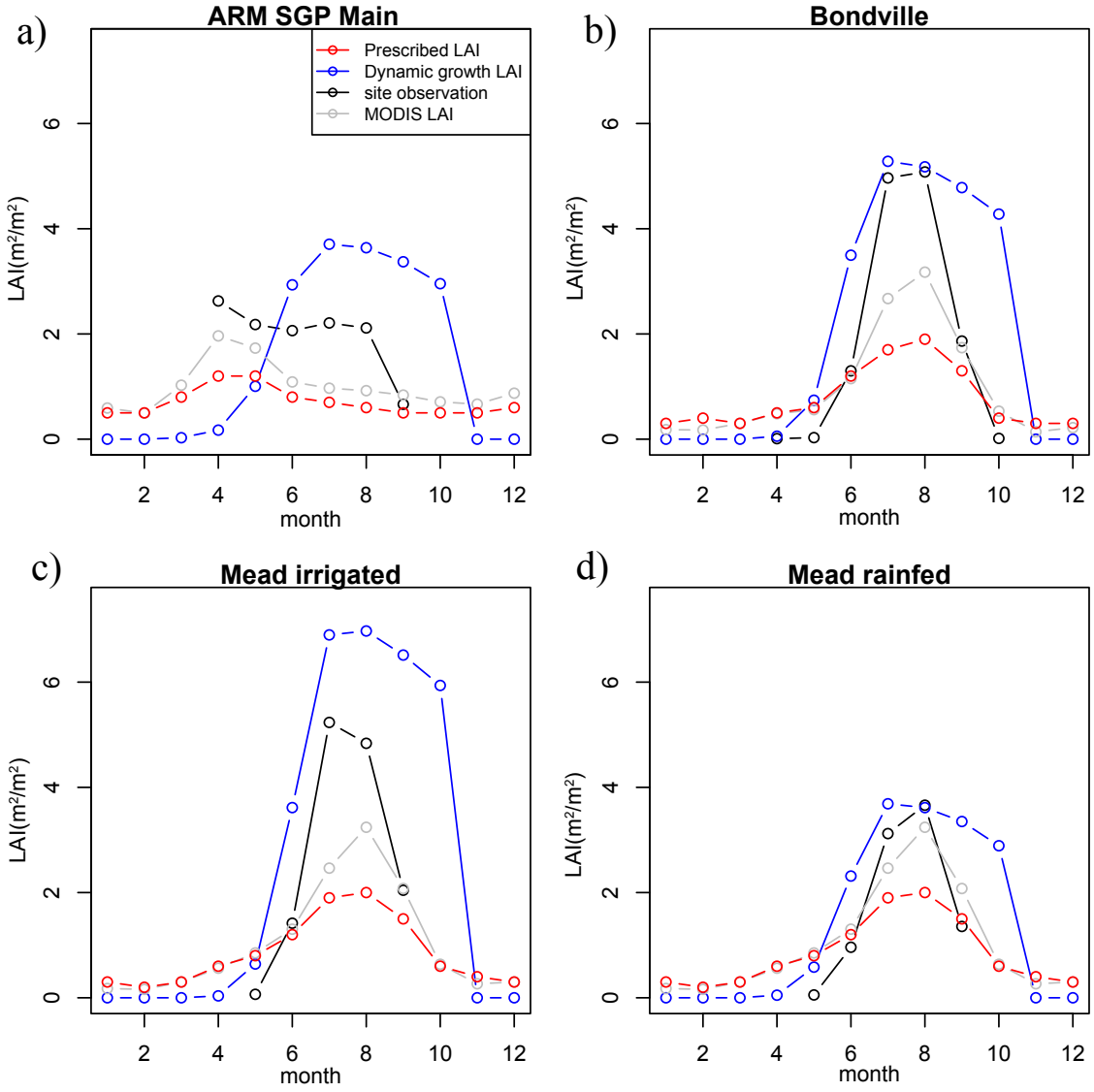

Figure 10. Simulated monthly LAI compared to observations at four AmeriFlux sites. Modeled and MODIS LAI are averaged for 2002-2011, and observed LAI is averaged for 2002-2010 for ARM SGP Main site, 2002-2007 for Mead irrigated and rainfed sites, and 1997-2001 for Bondville).

Although the dynamic crop simulation (CROP) overestimated peak LAI in some years, it captured the inter-annual variation in peak LAI better than the simulation with prescribed LAI (Figure 11), which has no interannual variation. MODIS LAI [*Zhu et al.*, 2012] underestimated peak LAI at the three sites by a magnitude similar to the overestimation by the CROP simulation. Irrigation reduced the inter-annual variability at Mead in the CROPIRR simulation, where the dynamic crop growth model showed larger variability at the rainfed site than at the irrigated site. But in observations, the variation in peak LAI at Mead rainfed is not as large as in the simulation. This may be because interannual variability in precipitation was overestimated (simulated standard deviation is 26.6% greater than observed).

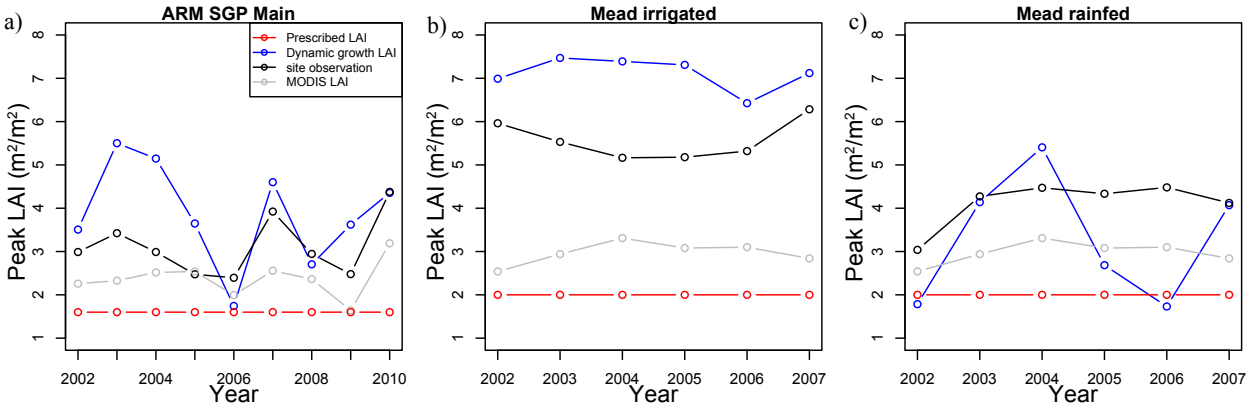

Figure 11. Variation in simulated annual peak LAI compared to three AmeriFlux sites

2) Planting date

We compared the planting date for C3 and C4 crops to observed soybean and maize planting dates [*Sacks et al.*, 2010]. Over 34.4% C3 and 61.5% C4 cropland, simulated planting dates were within the observed planting date range. For C3 cropland, the model simulated too-early planting by 5.7±0.4 days in the remaining 65.6% of C3 crop area. For C4 cropland, the model simulated too-early planting by 8.7±2.1 days in 37.4% of the C4 crop area, mostly in the Midwest and East. Only 1.1% of simulated C4 cropland had later than observed planting dates, by 10.4±3.4 days in Montana and Wyoming.

3) Surface climate

The CROP simulation overestimated mean daily temperature (Tmean; Figure 12a) in the Midwest by up to 4 ^{o}C with seasonal variation in the bias. The largest bias (+8 ^{o}C) was in July and smallest (+0.5 ^{o}C) was in March. The warm bias was reduced by 2-5 ^{o}C from the previous version of the coupled model [*Lu and Kueppers*, 2012]. Dew point temperature (Td) was underestimated in most regions (Figure 12b), indicating low humidity in the model simulations. Of 18% area of the entire U.S., such underestimation was strongly correlated ($r>0.8$) to the dry precipitation bias. Precipitation (ppt; Figure 12c) was underestimated in the Midwest and Eastern U.S. and overestimated in the Western U.S. by up to 2 mm day^{-1}. Where the model simulated excessive precipitation in the Western U.S., there was a cold bias and the low dew point temperature was due to underestimated air temperature.

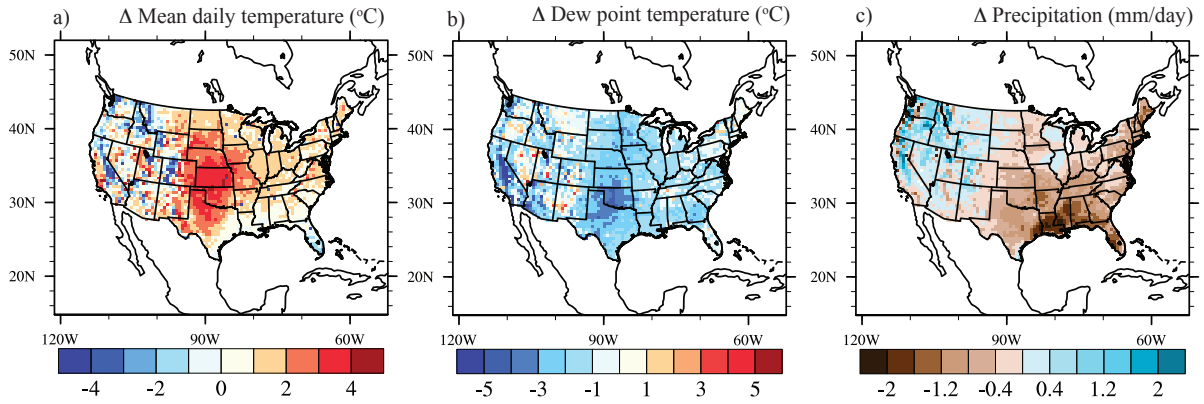

Figure 12. Averaged (2004-2006) difference between the CROP simulation and PRISM observations for (a) mean daily air temperature, (b) dew point temperature, and (c) precipitation.

The RMSE between PRISM and the four simulations (Table 5) indicated that adding both the dynamic crop model and the irrigation scheme slightly improved model simulation of temperature and precipitation. Adopting dynamic crop growth (CROP) reduced the RMSE by 5.6% on average for daily maximum temperature (Tmax), daily minimum temperature (Tmin), Tmean, and ppt compared to STD across all grid cells. Adding the irrigation scheme reduced the RMSE by 5.3% on average for Tmax, Tmin, Tmean, and ppt when comparing STD to STDIRR, and but only by 1.8% when comparing CROP to CROPIRR. The irrigation scheme reduced the RMSE not only in grid cells with irrigated cropland but also in grid cells with non-irrigated cropland. From STD to STDIRR, the RMSE decreased by 5.7% for irrigated cropland and by 7.5% for non-irrigated cropland. From CROP to CROPIRR, the RMSE decreased by 5.9% for irrigated cropland for Tmax, Tmin, Tmean, and Td and by 1.9% for non-irrigated cropland, but only for Tmin and Tmean.

Table 5. Spatially averaged Root Mean Square Error (RMSE) for maximum temperature (Tmax), minimum temperature (Tmin), mean temperature (Tmean), dew point temperature (Td), and precipitation (ppt) between PRISM and the four simulations (STD, STDIRR, CROP, and CROPIRR) in 2004-2006.

	All domain				Non-irrigated cropland				Irrigated cropland			
	STD	STDIRR	CROP	CROPIRR	STD	STDIRR	CROP	CROPIRR	STD	STDIRR	CROP	CROPIRR
Tmax (°C)	3.51	3.29	3.47	3.42	3.57	3.24	3.49	3.51	3.5	3.21	3.54	3.37
Tmin (°C)	2.82	2.68	2.53	2.47	2.43	2.27	2.01	1.97	3.27	3.06	2.83	2.67
Tmean (°C)	2.71	2.51	2.48	2.41	2.62	2.35	2.29	2.25	3.09	2.81	2.76	2.57
Td (°C)	2.7	2.76	2.71	2.69	2.35	2.42	2.28	2.37	2.78	2.74	2.78	2.61
ppt (mm/day)	1.25	1.22	1.22	1.22	1.32	1.27	1.28	1.29	1.29	1.25	1.27	1.27

4) Soil moisture

The coupled model generally over-predicted the soil moisture in the Western US and under-predicted soil moisture in the Midwest and Eastern US relative to site level

observations (Figure 13a). Adding the dynamic crop model did not improve the soil moisture simulation; at some sites, the low soil moisture bias was exacerbated because higher LAI in the dynamic crop model increased evapotranspiration over that in the prescribed crop (not shown). However, adding irrigation largely improved the soil moisture simulation at irrigated grid cells. At the Mead irrigated site, the simulation including both irrigation and dynamic crop growth best matched the observed soil moisture levels over the growing season (Figure 13b).

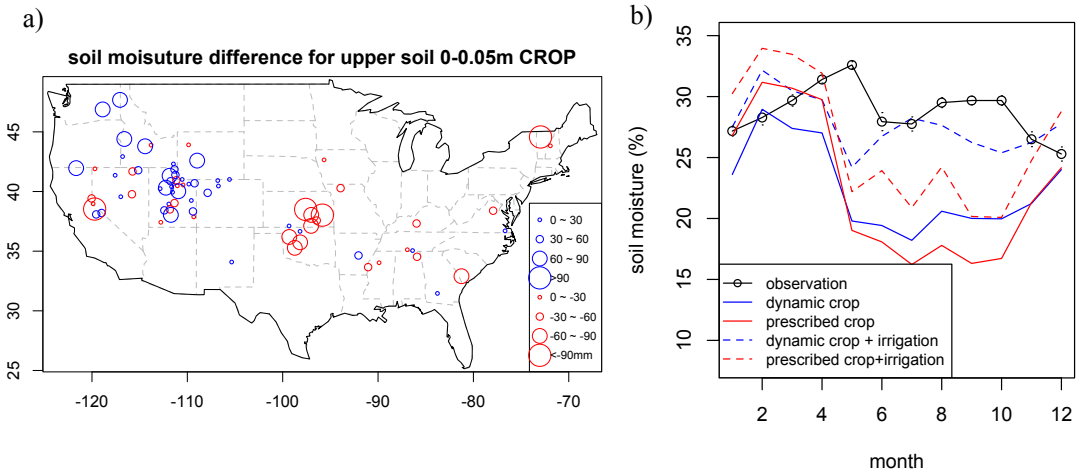

Figure 13. Comparison of simulated and observed soil moisture. a) Soil water (0-0.5m) difference between CROP and observed and b) soil moisture comparison at the Mead irrigated site.

5) Surface energy fluxes

Incorporating only dynamic crop growth does not substantially improve simulated surface energy fluxes, but the addition of irrigation does. Both STD and CROP simulated much higher sensible heat flux (H) than observed at all four Ameriflux sites (Figure 14) and did not capture the double peak pattern at Bo1 and Ne1. There was only slightly improvement in simulated H at Ro3 and Ne1 sites. At ARM and Bo1 sites, the CROP simulation actually produced higher H than STD, worsening the high bias. CROP simulated higher latent heat flux (LE) than STD, but still produced a peak in LE that was 1 to 2 months early at Ro3 and Bo1. With the addition of irrigation, biases in H and LE at the Mead irrigated site were reduced most in CROPIRR. The double peak pattern of H and the peak month of LE were well simulated by CROPIRR, but were not captured in STDIRR, which lacks a dynamic crop growth model.

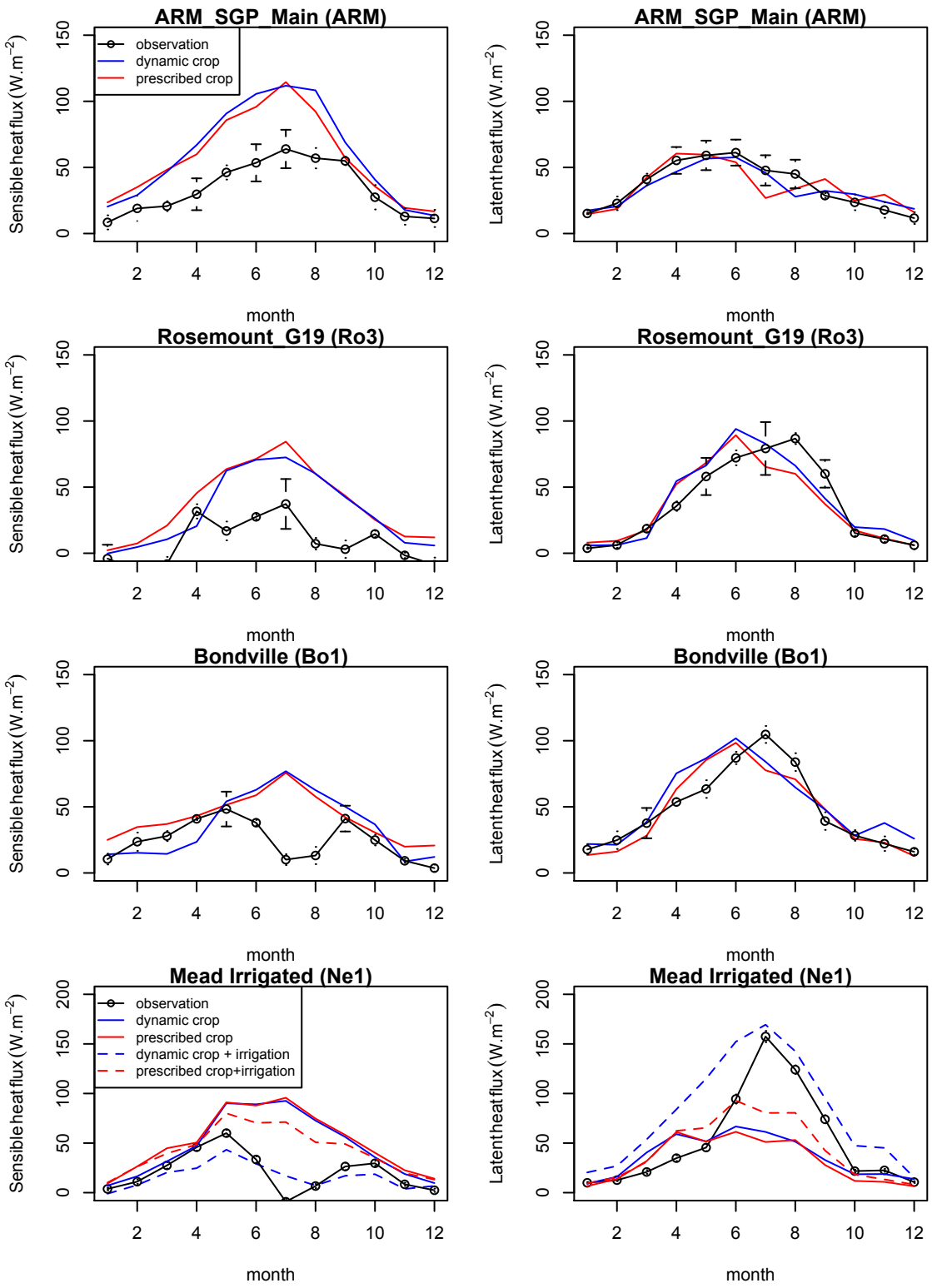

Figure 14. Comparisons of 2004-2006 monthly mean sensible heat flux (panel letters needed) and latent heat flux (panel letters needed) between model simulations and observations at four AmeriFlux sites.

The role of dynamic crop growth in climate effects of irrigation

We compared three years (2004-2006) difference in surface variables between the two sets of simulations to quantify how dynamic crop growth influences irrigation effects on surface energy fluxes and temperature. One set is CROPIRR and CROP that adopted dynamic crop growth, the other set is STDIRR and STD that used prescribed crop LAI.

Dynamic crop growth requires more irrigation water during the growing season than prescribed crop growth (Figure 15a). From April to September, the irrigation water applied in the CROPIRR simulation is almost double that in STDIRR. In winter, the simulation with prescribed crop had higher irrigation water (0.05 mm/day) because the dynamic crop module in CROP does not simulate winter crops or cover crops and therefore does not apply irrigation water from November to February. When comparing the two simulations with dynamic crop growth (CROPIRR and CROP), LAI was 32% greater with irrigation, while LAI did not change with irrigation under prescribed LAI (STDIRR and STD) (Figure 15b).

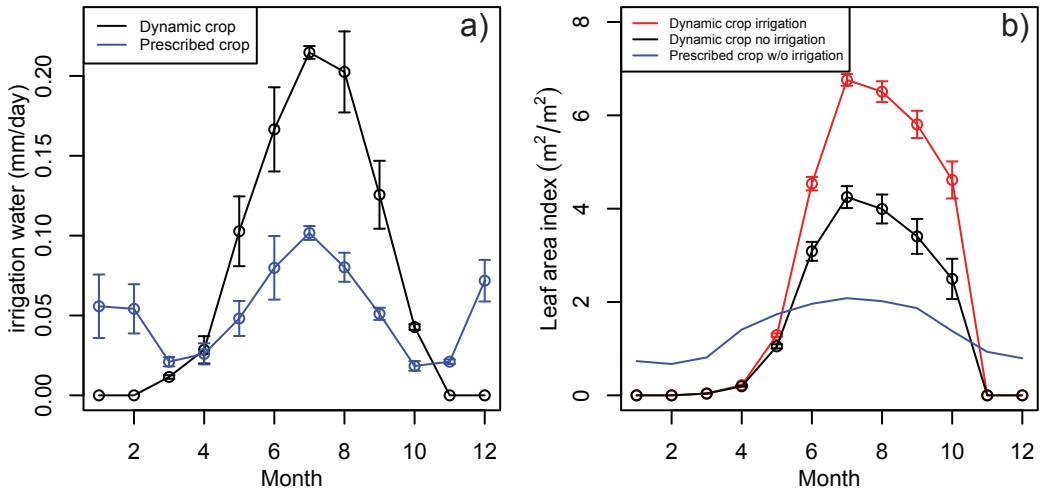

Figure 15. Monthly variation in domain averaged a) irrigation water (mm/day) and b) leaf area index (m2/m2) in prescribed crop and dynamic crop simulations.

Combined dynamic crop growth plus irrigation improved the simulated partitioning of latent heat flux. In CLM, the latent heat flux was partitioned into soil evaporation, wet leaf evaporation, and dry leaf transpiration. Because the LAI does not change with prescribed crop, a large fraction of the water applied to the soil column evaporated from the soil. In STDIRR, 50% of the total evapotranspiration was soil evaporation and 35% was leaf transpiration (Figure 16). In the simulation with dynamic crop growth, the increase in LE with irrigation is mainly due to increased leaf transpiration resulting from the larger leaf area; soil evaporation is only a small portion of LE.

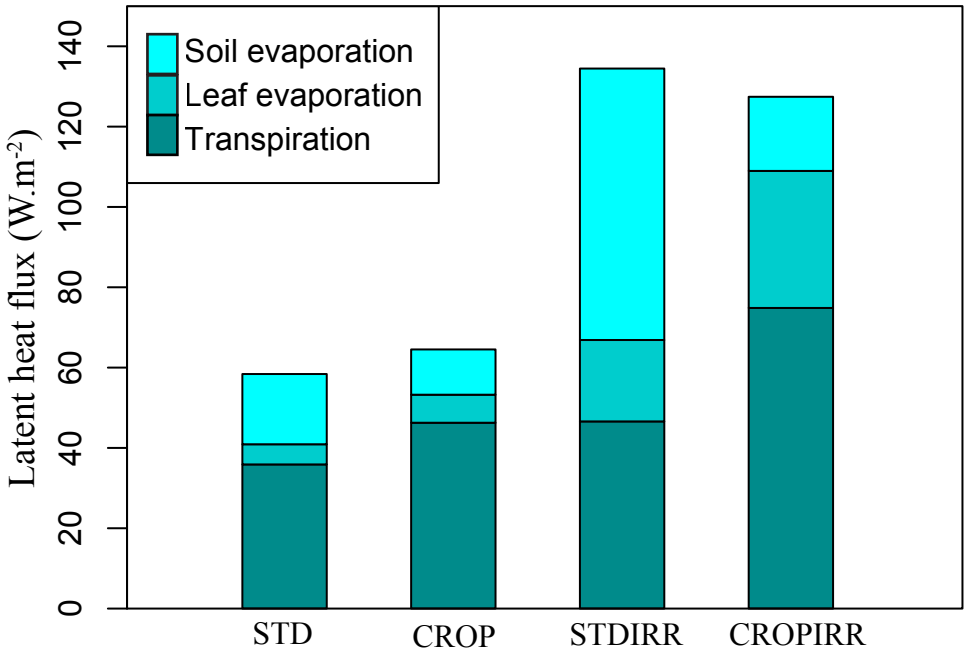

Figure 16. Simulated 2004-2006 averaged latent heat flux partitioned into three components for the four models.

The averaged JJA differences in climate variables with irrigation have a similar pattern but different magnitude in STDIRR and CROPIRR as the cell-fraction of irrigated cropland percentage increased (Figure 17). Irrigation increased LE while reduced H in both STDIRR and CROPIRR, and such effects is 34.6% higher for ΔH and 24.6% higher for ΔLE in CROPIRR with dynamic crop in moderately irrigated region (20-50% irrigated). Irrigation increased net radiation in a similar magnitude in STDIRR and CROPIRR except when irrigation land >60%, such increase in net radiation is 41.9% lower with dynamic crop. Irrigation reduced 2-meter air temperature (T2) stronger in CROPIRR than STDIRR when irrigated land >20%.

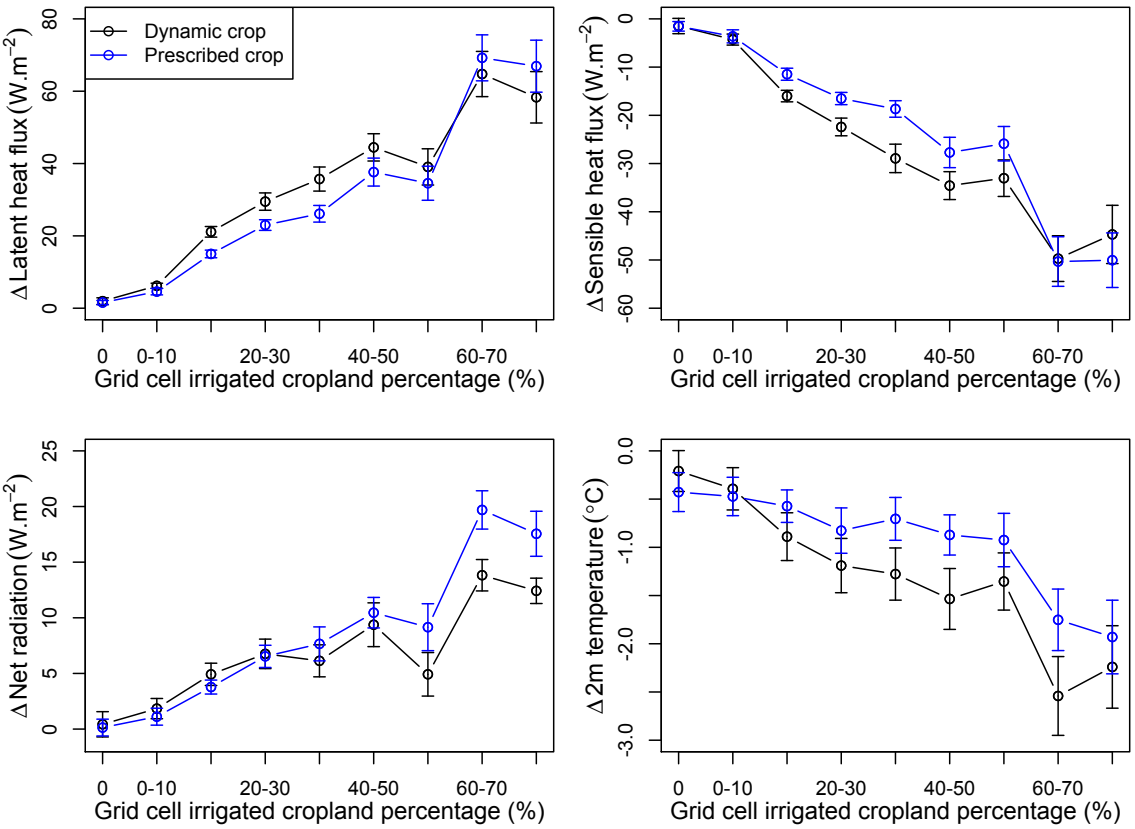

Figure 17. 2004-2006 JJA averaged difference along different grid cell irrigated cropland percentage of a) latent heat flux (W.m^{-2}), b) sensible heat flux (W.m^{-2}),c) net radiation (W.m-2) and d) 2m air temperature (°C) in prescribed crop and dynamic crop simulations. The error bar shows the standard error among 9 months.

Discussion and conclusion

Model evaluation

By coupling CLM4Crop into WRF (version 3.3), our work is a first step to extending the capability of WRF to simulate two-way interactions between crop growth and climate. As one of the most widely used regional climate models, standard versions of WRF do not include a comprehensive land surface model. Jin et al. [2010] first coupled the CLM (version 3) into WRF (version 2) and then Subin et al. [2011] updated the coupled model into a new version (WRF3.0-CLM3.5). We updated the coupled model to WRF3.3-CLM4 and incorporated a dynamic crop growth model to better reflect seasonal changes in LAI, and added an irrigation scheme to capture large effects of increased soil moisture on surface energy and water fluxes.

The surface energy flux evaluation suggested that improvements to dynamic crop growth are not sufficient to better simulate energy fluxes; improvements to other physical processes (such as precipitation) are equivalently important. We expected the larger and

more dynamic LAI simulated in CROP to improve simulation of surface energy fluxes where the prescribed LAI was small compared to observations. However, site-level comparisons to three non-irrigated AmeriFlux sites in the Midwest suggest that we did not realize the expected improvements. The reason may be that although the LAI is larger in CROP, the low precipitation bias persists, resulting in low soil moisture, limiting evapotranspiration regardless of the LAI. This also is accompanied by too low cloud cover and too large downward solar radiation, and net radiation. As a consequence, gross energy fluxes (e.g., latent heat flux, sensible heat flux) and the Bowen ratio have RMSEs in CROP comparable to those in STD at ARM and Bo1. At the Ne1 site, when irrigation was applied, surface energy flux partitioning was substantially improved. Therefore, we suspect that in regions with a dry bias, if the precipitation simulation could be improved, surface energy fluxes and flux partitioning will also improve.

While an improvement over previous versions, our evaluations revealed some of the improvement could because of incorrect reason. For example, in the previous version (WRF3.0-CLM3.5), there is a very large warm bias that up to 10 ^{o}C in the Midwest. Such warm bias in the Midwest was reduced by 2-3 ^{o}C when updating the land surface model as well as using MYNN boundary layer in STD and further reduced by 1-2 ^{o}C when adding dynamic crop growth model and irrigation practice. However, the overestimated LAI and longer growing season also contributed to the reduced warm bias in CROP and CROPIRR.

Comparing to CLM4CNCrop [*Levis et al.*, 2012], WRF3.3-CLM4crop has similar biases in crop growth even with modified carbon allocation parameters. Both models overestimated the LAI and growing season length. CLM4CNCrop simulated a higher LAI for soybean (C3 crop) than for maize (C4 crop); our model displayed similar results. Mean C3 LAI is greater than C4 LAI by 0.19 but with clear spatial variation (higher C3 LAI in the northern US and higher C4 LAI in the southern US). Excluding the soil carbon and nitrogen calculations from WRF3.3-CLM4crop limits its capability for studying biogeochemical interactions between cropland and climate. Levis et al. [2012] found adding dynamic crop growth resulted in the strongest improvements in simulation of biogeochemical variables (such as NEE) relative to biogeophysical variables (such as H and LE). Our current model can be only used to study biogeophysical interactions between climate and cropland. Furthermore, root distribution parameters [*Zeng*, 2001] were not updated as crops developed through the growing season in both models. Root carbon was simulated, but did not update the root distribution parameters. In future versions, a root growth submodel is needed to better capture the relationship between crop growth and root water uptake.

Irrigation increased latent heat flux (LE) comparably to other modeling studies that implemented precision irrigation schemes. Irrigation produced an increase in JJA LE of 21.4 W.m^{-2} under prescribed crop and 30.8 W.m^{-2} with dynamic crops over irrigated land. Harding and Snyder [2012] simulated an increase in JJA LE of 21 W.m^{-2} using standard WRF, Sacks et al. [2009] simulated an increase in JJA LE 20-30 W.m^{-2} using CCSM, and Cook et al. [2011] simulated an annual increase in LE by 16-20 W.m^{-2} using GISS ModelE. Previous work using simpler irrigation schemes produced much greater

increases in LE. For example, Kueppers et al. [2007b] simulated a 152 W.m^{-2} (20yr JJA average) increase in LE in California, and De Ridder and Gallee [1998] simulated a 75 W.m^{-2} (at midday) increase in LE in southern Israel. In observation, LE is 16.5 W.m^{-2} higher in JJA average at Mead irrigated than Mead rainfed site.

The role of dynamic crop growth in climate effects of irrigation

Our results suggest that the dynamic crop growth model is important for evaluation of crop management effects on climate. Without dynamic crop growth, models could underestimate the irrigation effects on climate in moderately irrigated regions. This is due to the amount of irrigation water applied. On average, simulations with dynamic crop growth required more irrigation water and therefore resulted in stronger increases in LE and decrease in H and T2 in moderately irrigated cropland. In addition, the dynamic crop growth simulation had a more reasonable simulation of latent heat flux components, with higher latent heat flux resulting from increased leaf evapotranspiration, not increased soil evaporation as occurred with prescribed LAI. The large soil evaporation is not reasonable because observations have shown that soil evaporation is about 30% of evapotranspiration for irrigated cropland [*Lascano et al.*, 1987].

Our simulation used a precision irrigation practice and the amount of annual irrigation water over the entire domain was validated with a USGS irrigation survey. However, the amount of water added to each state differed substantially from the USGS irrigation survey (Figure 18). This is due to model biases in soil moisture. For example, too much irrigation water was added to Texas and Nebraska in the model because the dry bias in this region resulted in insufficient soil water to support crop growth, while less irrigation water was applied in western states, such as California, Idaho, and Colorado due to the wet biases in these states. Therefore, ensemble simulations with multiple regional climate models and irrigation schemes may be required to accurately quantify effects of irrigation on surface climate.

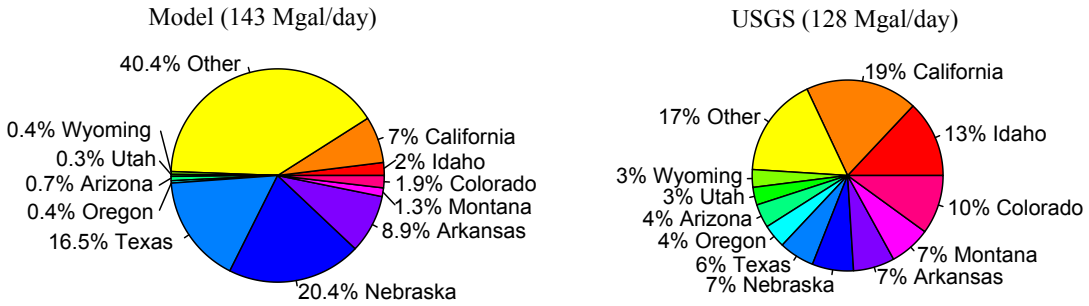

Figure 18. State level irrigation percentages for model (CROPIRR) and USGS in 2005. The total amount applied is 143 million gallons per day in CROPIRR, and 128 million gallons per day according to the USGS survey.

Conclusions

In summary, this work evaluated the performance of a coupled crop-climate model (WRF3.3-CLM4crop) in simulation of crop growth and surface climate. We found the coupled model overestimated crop leaf area index and growing season length but displayed a reasonable interannual variability. Adding both the dynamic crop model and the irrigation scheme improved model simulation of temperature and precipitation within and beyond agricultural regions. Adding irrigation reduced the dry bias at irrigated cropland and great improved the energy fluxes simulation at Mead irrigated site while the improvement was limited in other regions by the model's dry bias. A dynamic crop growth model is important for evaluation of crop management effects on climate. Excluding dynamic crop growth could under-predict effects in moderately irrigated regions, and could underestimated irrigation water demands.

CHAPTER 3

Increased heat waves with loss of irrigation in United States

Introduction

Long-term temperature observations have indicated an increased frequency and intensity of heat waves since the 1950s [*Gaffen and Ross*, 1998; *IPCC*, 2007], resulting in higher heat-related mortality and other public health challenges. For example, there were at least 700 excess deaths during the 1995 Chicago heat waves [*Semenza et al.*, 1996], and 15,000 excess deaths during the 2003 heat waves in France [*Fouillet et al.*, 2006]. More frequent and hotter heat waves can also increase heat stress in livestock, wildlife, crops, and forests [*Ciais et al.*, 2005; *Hahn*, 1999; *van der Velde et al.*, 2010] and therefore affect regional economies and ecosystems [*Jolly et al.*, 2005; *Reusch et al.*, 2005]. Projections of future climate using global climate models suggest more heat waves over nearly all land areas [*IPCC*, 2007]. Therefore, understanding factors that contribute to heat waves is becoming increasingly important for impact prediction and decision-making.

Human activities are contributing to the increased frequency and intensity of heat waves. Many studies have shown that industrial greenhouse gas emissions increase both global mean temperature and heat index of heat waves [*Karoly et al.*, 2003; *Stott et al.*, 2004; *Tett et al.*, 1999], yet land use and land use change can also alter heat waves at the regional scale. Urban heat islands exacerbated the impact of heat waves in the Midwest in 1995 [*Kunkel et al.*, 1996] and historical meteorological data indicates that agricultural irrigation raised the dew point temperature during heat waves in Chicago [*Changnon et al.*, 2003]. With the same air temperature, higher dew point temperature can increase the apparent temperature [*Steadman*, 1984] resulting in greater mortality and severe human health effects [*Conti et al.*, 2005; *Naughton et al.*, 2002; *Smoyer*, 1998].

Irrigation has been found to alter climate at global and regional scales [*Adegoke et al.*, 2003; *Cook et al.*, 2011; *Harding and Snyder*, 2012; *Jin and Miller*, 2011; *Ozdogan and Salvucci*, 2004; *Sorooshian et al.*, 2011]. The extra water applied to the soil enhances evapotranspiration, thereby reducing surface temperature through evaporative cooling [*Kueppers et al.*, 2007b; *Lobell et al.*, 2009; *Sacks et al.*, 2009]. Condensation of the water vapor in the atmosphere releases latent heat that provides energy for cloud convection and precipitation [*DeAngelis et al.*, 2010; *Saeed et al.*, 2009], an effect that can propagate to neighboring regions [*Lo and Famiglietti*, 2013]. The surface cooling reduces emission of surface long wave radiation, while the water vapor in the upper air can absorb and release more long wave radiation to the surface [*Boucher et al.*, 2004; *Kueppers and Snyder*, 2012], thereby increasing the surface net radiation. Irrigation also can increase net solar radiation at the surface due to the decreased albedo of wet soil [*Otterman*, 1977]. However, there have been few studies of the effects of irrigation on

temperature extremes [*Lobell et al.*, 2008a] and the degree to which irrigation affects heat wave frequency, duration, and intensity is not well studied.

In this paper, we analyze the effects of irrigation on heat waves in the contiguous United States using a newly coupled regional climate-land surface model (WRF3.3-CLM4crop), which includes a weather-sensitive irrigation scheme and dynamic crop growth. A key issue is that the simulation models used to explore the irrigation effects typically have prescribed crop leaf area values that do not respond to environmental change or inter-annual variation in weather and climate. This prescribed approach could overestimate and underestimate evapotranspiration from croplands, depending on time of year and environmental conditions, because crop leaf area and physiological activity are known to dynamically respond to climate variation [*Fang et al.*, 2001; *Porter and Semenov*, 2005]. In our simulations, crop growth in the model depends on growing season temperatures and soil moisture, and better captured interannual variability in crop growth. We also adopted a diversity of heat wave indices because variation in definition resulted in different geographic distributions. As pointed out by Smith et al. (2013), climate researchers use a statistical quartile from a period of climate data as a threshold to detect heat waves, while health researchers use absolute critical temperature values that could result in human death to determine heat waves. Therefore, we adopted the same fifteen heat wave definitions to quantify responses important both for climate and human health.

Methods

We performed two 10-year (2002-2011) simulations using WRF3.3-CLM4crop to evaluate irrigation effects on heat waves. One is a control simulation without irrigation (hereafter referred to as CROP), and the other includes irrigation (hereafter referred to as CROPIRR). The physical modules used in all simulations include the MYNN boundary layer scheme [*Nakanishi and Niino*, 2006], the CAM longwave/shortwave radiation scheme [*Collins et al.*, 2004], the new Grell cumulus scheme [*Grell and Devenyi*, 2002], and the Thompson microphysics scheme [*Thompson et al.*, 2004]. The simulations focused on the continental United States (U.S.) with 25 vertical layers and 50 km horizontal resolution. We interpolated (using the inverse distance weighting method) 0.5 deg CLM surface input data (including plant functional types, plant function type percent, leaf area index, and stem area index) into the model domain. We used NCEP/DOE Reanalysis II data as lateral boundary conditions [*Kanamitsu et al.*, 2002]. For analysis, we removed 8 grid cells from the full perimeter of the domain as a buffer, which diminished the original domain from 109 ×129 to 93×113 grid cells. The first two years of the simulations were discarded as spin-up and the analysis focused on the final 8 years (2004-2011).

We adopted a precision agriculture-type irrigation scheme, where the amount and timing of irrigation simulates efficient irrigation practices. Irrigation water is applied as a function of root water stress (β_t), leaf temperature (T_{veg}) and LAI. The root water stress is monitored by β_t, which varies from near zero (dry soil) to one (wet soil). Leaf temperature also is used, not only to more realistically simulate irrigation systems [*Howell et al.*, 1984; *Wanjura et al.*, 1992], but also to maintain optimum plant growth

because high leaf temperature can inhibit plant photosynthesis [*Wise et al.*, 2004]. Irrigation starts after leaf emergence (LAI>0.1 m^2 m^{-2}), and occurs when either plant water is low ($\beta_t < 0.99$) or leaf temperature is too high (T_{veg} >35°C). Irrigation water is applied in the form of rain at a constant rate of 0.0002 mm s^{-1}, selected to match the range of current irrigation systems (4-20 gallons per minute per acre). Cropland equipped for irrigation was derived from the 0.05 deg global irrigation map [*Siebert et al.*, 2005], as updated in 2006 (http://www.geo.uni-frankfurt.de/ipg/ag/dl/forschung/Global_Irrigation_Map/index.html). The simulated annual irrigation water use (Figure 9b) is within 14% of U.S. water usage estimated by USGS for 2005 [*Kenny et al.*, 2005]. The range in annual simulated irrigation water use from 2004-2006 was 113-149 billion gallons per day (143 for 2005); the USGS survey estimates 128 billion gallons per day in 2005 (http://ga.water.usgs.gov/edu/wuir.html).

We analyzed irrigation effects on fifteen heat wave indices (HINs) summarized in Smith et al. (2013) Table 1 (Table S1 in Appendix B). We also used the daily mean heat index [*Schoen*, 2005] during a heat wave to represent the intensity of the heat wave because it shows both temperature and humidity effects. The heat index is defined as:

$$HI = T - 1.0799e^{0.03755T}[1 - e^{0.0801(D-14)}]$$

where T is temperature and D is dew point temperature at the lowest atmosphere layer. We compared 8-year (2004-2011) differences (CROPIRR-CROP) in heat wave frequency (number of heat waves per year), duration (number of consecutive days comprising each heat wave), and intensity to quantify irrigation effects on heat waves. We discuss statistically significant results based on a student t test (n=24, which includes JJA in the 8 years, $p<0.05$).

Results

Most HINs showed significant irrigation effects on heat waves in the California's Central Valley and the Southern High Plains (Figure 19). Heat wave frequency and duration was significantly decreased with irrigation in the California's Central Valley and the Southern High Plains for up to 8 out of 15 HINs (Figure S1 in Appendix B). The highest reduction of frequency was found in the Southern High Plain by 2 events/year. Conversely, heat wave intensity was significantly increased in California's Central Valley and the Southern High Plains for 7 out of 15 HINs by 0.2-1.0 ^{o}C. Irrigation reduced heat wave frequency and duration because its cooling effects made fewer days exceed the threshold. Increased heat wave intensity with irrigation is because the dew point temperature increased further than the air temperature was reduced. Although irrigation significantly increased heat wave frequency and duration in some grid cells, the spatial distribution is scattered and not consistent for the 15 HINs, perhaps due to the remote impact of the atmospheric circulation.

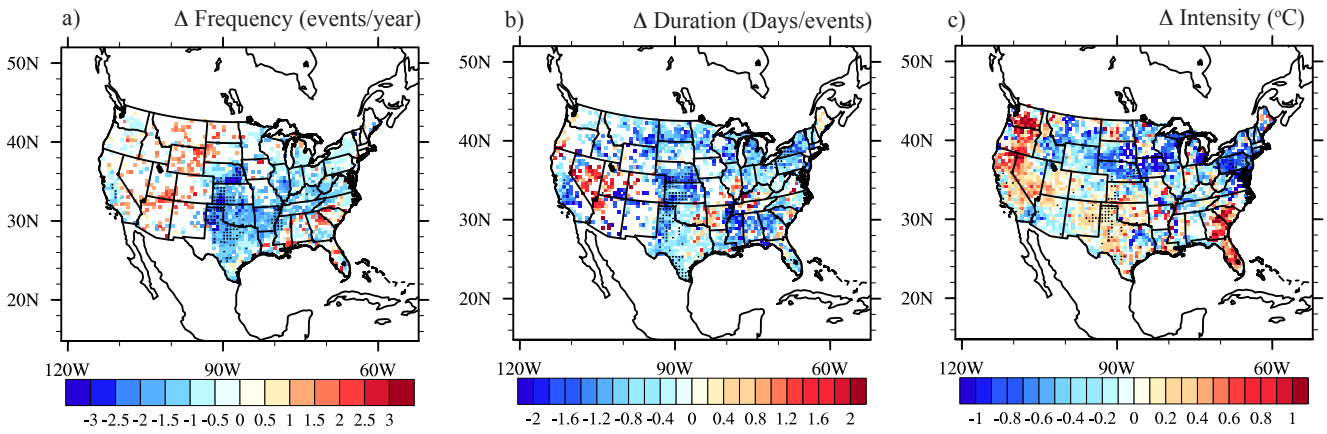

Figure 19. The 8-year (2004-2011) averaged significant difference (CROPIRR-CROP) of heat wave frequency, duration, and intensity. We showed all significant difference (t-test, n=24, $p<0.05$) for the fifteen indices on a same map. For a grid cell that have significant different for more than one index, we averaged the difference across the indices. The stippled area indicated the significant difference in more than five heat wave indices. The significant differences for each heat wave index were showed in supplement figures S1-3.

The fifteen HINs resulted in divergent irrigation effects on heat waves as irrigated percent increased (Figure 20). Most HINs were more strongly affected as irrigated percent increased and effects were strongest with irrigated percentage >50%. Across all of the HINs, irrigation consistently decreased heat wave durations, while effects on frequency and intensity were inconsistent across HINs. In intensively irrigated cropland (irrigated percent >50%), irrigation reduced duration by 0.1-2.6 days/event across all HINs. While irrigation increased heat wave frequency by 0.1-1.0 events/year for 3 HINs, it decreased frequency by 0.1-4.2 events/year for the other 12 HINs. Heat wave intensity increased by 0.05-1.8 ^{o}C for 7 HINs but decreased by 0.05-0.8 ^{o}C for the other 8 HINs. Averaged over all HINs, irrigation reduced heat wave frequency and duration, but increased intensity.

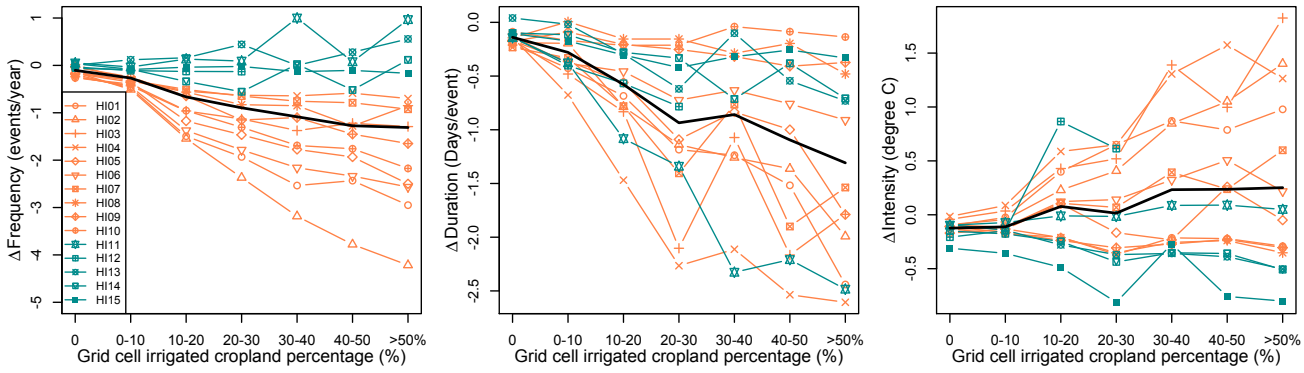

Figure 20. The 8-year (2004-2011) averaged difference (CROPIRR-CROP) of heat wave frequency, duration, and intensity for fifteen heat wave indices as grid cell irrigated cropland percentage increasing. We colored the indices use relative and absolute

threshold as orange and green respectively. The black line indicates the average over the 15 indices.

Discussion and conclusions

Our primary goal was to evaluate irrigation effects on heat wave frequency, duration, and intensity across a diversity of climatological and health-related heat wave definitions. Irrigation effects on heat waves were statistically significant over irrigated cropland, but the effects were not significant in non-irrigated regions. Effect size, and in some cases sign, varied across the fifteen HINs evaluated. However, on average across all HINs, irrigation reduced heat wave frequency and duration, but increased intensity in our model. These effects were greater as the percent of land area that was irrigated in a model grid cell increased.

The model produced too many heat wave days for all fifteen heat wave indices due to a persistent warm bias (Lu et al. in prep). The number of heat wave days derived from CROPIRR was higher than that found by Smith et al. (2013) using the North American Land Data Assimilation System (NLDAS-2) dataset. Whether the overestimated heat wave baseline affects our estimate of irrigation effects on heat waves (difference between CROPIRR and CROP) is unknown. However, evaluation of the coupled model (Lu et al., manuscript) indicated that by implementing dynamic crop growth, model performance is improved over prior versions. Further, the increase in latent heat flux due to irrigation is comparable to other models results and observations. Therefore, although the actual magnitude may differ from what is represented in the model, the pattern should be qualitatively correct.

Using fifteen different heat wave indices extended our understanding of how irrigation affects heat waves. In particular, the heat index temperature metric has a larger impact on the index's sensitivity to irrigation than does the threshold percentile. For example, irrigation increased heat wave intensity for HI01-HI04 (mean daily temperature metric) but decreased heat wave intensity for HI08-10 (maximum daily apparent temperature metric). Using the same temperature matric but different threshold percentiles resulted in qualitatively similar irrigation effects on heat waves. For example, irrigation reduced heat wave frequency for HI01-HI04 significantly in California central valley and south high plain, although the magnitude decreasing as the percentile increasing. Furthermore, we found the climatological heat wave indices (i.e. the relative indices) are more sensitive to irrigation than the health related indices (i.e. the absolute indices). More area showed significant difference for HI01-10 than HI11-15, and the magnitude of the differences are higher as well.

The southern high plains are most likely to suffer more and longer heat waves if there is a reduction in irrigation due to groundwater depletion. Although both California's Central Valley and Southern High Plains are experiencing groundwater deficits (Famiglietti and Rodell 2013) and they both displayed significant changes in heat waves with irrigation, Scanlon et al. [2012] suggest that the groundwater in the Central Valley is renewable

through artificial recharge with excess surface water. However, in the Southern High Plains, 35% of the area will be unable to support irrigation within the next 30 years under current depletion rates [*Scanlon et al.*, 2012]. Our results indicate that such declines in irrigation will lead to an increase of heat wave frequency and duration, exacerbating anticipated increases in temperature due to global climate change. Therefore, sustainable irrigation and adaptation are required in the regions not only to overcome direct drought damages, but also to diminish the potential climate consequences of less irrigation.

Conclusion

My work demonstrated the comprehensive land surface model that incorporated the dynamic crop model and irrigation could improve the surface energy fluxes simulation. In the first chapter, the analyses show that WRF3-CLM3.5 output is in good agreement with observed energy partitioning over needleleaf evergreen forests, but has errors in cropland, grassland and broadleaf deciduous forest. The poor energy flux simulations in cropland worsen the warm bias in the Midwest. So in the second chapter, I updated the coupled model to WRF3.3-CLM4crop that incorporated the dynamic crop model and irrigation. Comparison to one AmeriFlux site confirmed that when irrigation and dynamic crop growth were both applied, surface energy flux partitioning was substantially improved. However, the improvement over non-irrigated cropland was limited by the dry bias. Although the LAI is larger, the low precipitation bias persists, resulting in low soil moisture, limiting evapotranspiration regardless of the LAI, and hence still overestimated sensible heat flux and underestimated latent heat flux. Efforts to improve crop surface energy flux simulations also apply to other vegetation types. Solving the model dry bias before adding a dynamic vegetation model is likely to be more fruitful. Unlike crops that may be irrigated, natural grass land and forest depend on precipitation. Although a dynamic vegetation model may improve the leaf area index simulation, improvement of the surface energy fluxes could be limited by the dry bias.

The improved surface energy fluxes, particularly the higher latent heat flux, reduced the warm bias in the Midwest. In the previous version (WRF3.0-CLM3.5), there is a very large warm bias of up to 10 ^{o}C in the Midwest due to the deficiencies in both WRF and CLM. Such a warm bias in the Midwest was reduced by 2-3 ^{o}C when updating the land surface model as well as using MYNN boundary layer in WRF3.3 and further reduced by 1-2 ^{o}C when adding dynamic crop growth model and irrigation. However, some of the improvement may also be due to new errors introduced by the dynamic crop model. For example, the overestimated LAI and longer growing season also contributed to the reduced warm bias. Even with these changes, the warm bias in the Midwest still exists. The downward solar radiation bias contributes substantially to the warm bias. Reducing downward solar radiation is not simple because it is associated with many factors. Previous work [*Markovic et al.*, 2008; *Wild et al.*, 2001] suggests the overestimate of downward solar radiation at the surface could be either due to less cloud cover for cloudy days or less sky absorption of downward solar radiation for clear days. Ignoring aerosols in the model may also contribute to excess downward solar radiation [*Wild*, 2008]. And there could be other reasons not yet detected also contributing to the warm bias.

The bias in temperature and soil moisture produced errors in the dynamic crop growth and irrigation schemes. Crop growth depends on growing degree days. The warm bias accelerated accumulation of growing degree days. The differences in the crop phenology need to be quantified in a future version when crop phenology survey data are available. Accurately simulating irrigation amount is also limited by the warm bias. Our simulation used a precision irrigation practice and the amount of annual irrigation water over the entire domain was validated with a USGS irrigation survey. However, the amount of

water added to each state differed substantially from the USGS irrigation survey. This is due to model biases in soil moisture. For example, too much irrigation water was added to Texas and Nebraska in the model because the dry bias in this region resulted in insufficient soil water to support crop growth, while less irrigation water was applied in western states, such as California, Idaho, and Colorado due to the wet biases in these states.

There are several limitations of the coupled model that need to be resolved in the future version. Excluding the soil carbon and nitrogen calculations from WRF3.3-CLM4crop limits its capability for studying biogeochemical interactions between cropland and climate. Levis et al. [2012] found adding dynamic crop growth resulted in stronger improvements in simulation of biogeochemical variables (such as NEE) relative to biogeophysical variables (such as H and LE). Our current model only can be used to study biogeophysical interactions between climate and cropland. Furthermore, root distribution parameters [*Zeng*, 2001] were not updated as crops developed through the growing season in both models. Root carbon was simulated, but did not update the root distribution parameters. In future versions, a root growth submodel is needed to better capture the relationship between crop growth and root water uptake.

My work suggests that the dynamic crop growth model is important for evaluation of crop management effects on climate. Without a dynamic crop growth, climate models could underestimate the irrigation effects on temperature in moderately irrigated regions, which is due to the amount of irrigation water applied. On average, simulations with dynamic crop growth required more irrigation water and therefore resulted in stronger increases in LE and decrease in H and T2 in moderately irrigated cropland. In addition, dynamic crop growth showed a more reasonable simulation of latent heat flux components, with higher latent heat flux resulting from increased leaf evapotranspiration, not increased soil evaporation as occurred with prescribed LAI. Beside irrigation, the study of other crop management practices may also need dynamic crop growth. For example, the time to apply cover crop or conservation tillage is related to crop planting and harvest date that varies each year.

The coupled model has many potential applications in studying the interaction between climate and agriculture. The third chapter showed one application of WRF3.3-CLM4crop in studying the irrigation effects on heat waves. The results showed irrigation effects on heat waves were statistically significant over irrigated cropland, but the effects were not significant in non-irrigated regions. On average across all fifteen heat wave definitions, irrigation reduced heat wave frequency and duration, but increased intensity in our model. These effects were greater as the percent of land area that was irrigated in a model grid cell increased. Beside this application, the coupled model has other potential applications, such as how climate variability changes the crop growth, how the expansion of cropland affects climate, and the irrigation requirement in future climate scenarios.

REFERENCES

Adams, R. M., C. Rosenzweig, R. M. Peart, J. T. Ritchie, B. A. Mccarl, J. D. Glyer, R. B. Curry, J. W. Jones, K. J. Boote, and L. H. Allen (1990), Global Climate Change and United-States Agriculture, *Nature*, *345*(6272), 219-224.

Adegoke, J. O., R. Pielke, and A. M. Carleton (2007), Observational and modeling studies of the impacts of agriculture-related land use change on planetary boundary layer processes in the central US, *Agr Forest Meteorol*, *142*(2-4), 203-215.

Adegoke, J. O., R. A. Pielke, J. Eastman, R. Mahmood, and K. G. Hubbard (2003), Impact of irrigation on midsummer surface fluxes and temperature under dry synoptic conditions: A regional atmospheric model study of the U.S. high plains, *Mon Weather Rev*, *131*(3), 556-564.

Ainsworth, E. A., and S. P. Long (2005), What have we learned from 15 years of free-air CO2 enrichment (FACE)? A meta-analytic review of the responses of photosynthesis, canopy, *New Phytologist*, *165*(2), 351-371.

Ainsworth, E. A., et al. (2002), A meta-analysis of elevated [CO2] effects on soybean (Glycine max) physiology, growth and yield, *Global Change Biology*, *8*(8), 695-709.

Amthor, J. S. (2003), Effects of atmospheric CO2 concentration on wheat yield: review of results from experiments using various approaches to control CO2 concentration (vol 73, pg 1, 2001), *Field Crops Research*, *84*(3), 395-395.

Aoki, M., and K. Yabuki (1977), Studies on Carbon-Dioxide Enrichment for Plant-Growth .7. Changes in Dry-Matter Production and Photosynthetic Rate of Cucumber during Carbon-Dioxide Enrichment, *Agr Meteorol*, *18*(6), 475-485.

Augustine, J. A., J. J. DeLuisi, and C. N. Long (2000), SURFRAD - A national surface radiation budget network for atmospheric research, *Bulletin of the American Meteorological Society*, *81*(10), 2341-2357.

Baldocchi, D., et al. (2001), FLUXNET: A new tool to study the temporal and spatial variability of ecosystem-scale carbon dioxide, water vapor, and energy flux densities, *Bulletin of the American Meteorological Society*, *82*(11), 2415-2434.

Bonan, G. B. (2008), Forests and climate change: Forcings, feedbacks, and the climate benefits of forests, *Science*, *320*(5882), 1444-1449.

Bonan, G. B., K. W. Oleson, M. Vertenstein, S. Levis, X. B. Zeng, Y. J. Dai, R. E. Dickinson, and Z. L. Yang (2002), The land surface climatology of the community land model coupled to the NCAR community climate model, *Journal of Climate*, *15*(22), 3123-3149.

Bondeau, A., P. C. Smith, S. Zaehle, S. Schaphoff, W. Lucht, W. Cramer, and D. Gerten (2007a), Modelling the role of agriculture for the 20th century global terrestrial carbon balance, *Global Change Biology*, ***13***(**3**), **679-706**.

Bondeau, A., et al. (2007b), Modelling the role of agriculture for the 20th century global terrestrial carbon balance, *Global Change Biology*, *13*(3), 679-706.

Bonfils, C., and D. Lobell (2007), Empirical evidence for a recent slowdown in irrigation-induced cooling, *Proceedings of the National Academy of Sciences of the United States of America*, *104*(34), 13582-13587.

Bonhomme, R. (2000), Bases and limits to using 'degree.day' units, *European Journal of Agronomy*, *13*(1), 1-10.

Boucher, O., G. Myhre, and A. Myhre (2004), Direct human influence of irrigation on atmospheric water vapour and climate, *Climate Dynamics*, *22*(6-7), 597-603.

Bounoua, L., R. DeFries, G. J. Collatz, P. Sellers, and H. Khan (2002), Effects of land cover conversion on surface climate, *Climatic Change*, *52*(1-2), 29-64.

Brown, R. A., and N. J. Rosenberg (1999), Climate change impacts on the potential productivity of corn and winter wheat in their primary United States growing regions, *Climatic Change*, *41*(1), 73-107.

Butterfield, R. E., and J. I. L. Morison (1992), Modeling the Impact of Climatic Warming on Winter Cereal Development, *Agr Forest Meteorol*, *62*(3-4), 241-261.

Changnon, D., M. Sandstrom, and C. Schaffer (2003), Relating changes in agricultural practices to increasing dew points in extreme Chicago heat waves, *Climate Research*, *24*(3), 243-254.

Chen, F., and J. Dudhia (2001), Coupling an advanced land surface-hydrology model with the Penn State-NCAR MM5 modeling system. Part I: Model implementation and sensitivity, *Monthly Weather Review*, *129*(4), 569-585.

Chou, M.-D., and M. J. Suarez (1994), An efficient thermal infrared radiation parameterization for use in general circulation models, *Rep. NASA Tech. Memo 104606*, 85 pp, NASA Goddard Space Flight Center, Greenbelt, Md.

Ciais, P., et al. (2005), Europe-wide reduction in primary productivity caused by the heat and drought in 2003, *Nature*, *437*(7058), 529-533.

Collins, W. D., et al. (2004), Description of the NCAR Community Atmosphere Model (CAM 3.0), *Rep. NCAR/TN-464+STR*, 226 pp.

Conti, S., P. Meli, G. Minelli, R. Solimini, V. Toccaceli, M. Vichi, C. Beltrano, and L. Perini (2005), Epiderniologic study of mortality during the Summer 2003 heat wave in Italy, *Environmental Research*, *98*(3), 390-399.

Cook, B. I., M. J. Puma, and N. Y. Krakauer (2011), Irrigation induced surface cooling in the context of modern and increased greenhouse gas forcing, *Climate Dynamics*, *37*(7-8), 1587-1600.

Cooper, R. L., and W. A. Brun (1967), Response of Soybeans to a Carbon Dioxide-Enriched Atmosphere, *Crop Sci*, *7*(5), 455-&.

Covell, S., R. H. Ellis, E. H. Roberts, and R. J. Summerfield (1986), The Influence of Temperature on Seed-Germination Rate in Grain Legumes .1. A Comparison of Chickpea, Lentil, Soybean and Cowpea at Constant Temperatures, *Journal of Experimental Botany*, *37*(178), 705-715.

Cox, P. M., R. A. Betts, C. D. Jones, S. A. Spall, and I. J. Totterdell (2000), Acceleration of global warming due to carbon-cycle feedbacks in a coupled climate model, *Nature*, *408*(6809), 184-187.

Davin, E. L., and N. de Noblet-Ducoudre (2010), Climatic Impact of Global-Scale Deforestation: Radiative versus Nonradiative Processes, *Journal of Climate*, *23*(1), 97-112.

De Ridder, K., and H. Gallee (1998), Land surface-induced regional climate change in southern Israel, *Journal of Applied Meteorology*, *37*(11), 1470-1485.

DeAngelis, A., F. Dominguez, Y. Fan, A. Robock, M. D. Kustu, and D. Robinson (2010), Evidence of enhanced precipitation due to irrigation over the Great Plains of the United States, *J Geophys Res-Atmos*, *115*.

Di Luzio, M., G. L. Johnson, C. Daly, J. K. Eischeid, and J. G. Arnold (2008), Constructing retrospective gridded daily precipitation and temperature datasets for the conterminous United States, *Journal of Applied Meteorology and Climatology*, *47*(2), 475-497.

Diffenbaugh, N. S. (2009), Influence of modern land cover on the climate of the United States, *Climate Dynamics*, *33*(7-8), 945-958.

Diffenbaugh, N. S., T. W. Hertel, M. Scherer, and M. Verma (2012), Response of corn markets to climate volatility under alternative energy futures, *Nat Clim Change*, *2*(7), 514-518.

Dirmeyer, P. A., F. J. Zeng, A. Ducharne, J. C. Morrill, and R. D. Koster (2000), The sensitivity of surface fluxes to soil water content in three land surface schemes, *Journal of Hydrometeorology*, *1*(2), 121-134.

Easterling, W. E., N. J. Rosenberg, M. S. Mckenney, C. A. Jones, P. T. Dyke, and J. R. Williams (1992), Preparing the Erosion Productivity Impact Calculator (Epic) Model to Simulate Crop Response to Climate Change and the Direct Effects of Co2, *Agr Forest Meteorol*, *59*(1-2), 17-34.

Ericsson, T., L. Rytter, and E. Vapaavuori (1996), Physiology of carbon allocation in trees, *Biomass Bioenerg*, *11*(2-3), 115-127.

Fang, J. Y., S. L. Piao, Z. Y. Tang, C. H. Peng, and J. Wei (2001), Interannual variability in net primary production and precipitation, *Science*, *293*(5536), U1-U2.

Feddema, J. J., K. W. Oleson, G. B. Bonan, L. O. Mearns, L. E. Buja, G. A. Meehl, and W. M. Washington (2005), The importance of land-cover change in simulating future climates, *Science*, *310*(5754), 1674-1678.

Fischer, M. L. (2005), Carbon Dioxide Flux Measurement Systems Handbook, *Rep. ARM TR-048*.

Foley, J. A., et al. (2005), Global consequences of land use, *Science*, *309*(5734), 570-574.

Fouillet, A., G. Rey, F. Laurent, G. Pavillon, S. Bellec, C. Guihenneuc-Jouyaux, J. Clavel, E. Jougla, and D. Hemon (2006), Excess mortality related to the August 2003 heat wave in France, *International Archives of Occupational and Environmental Health*, *80*(1), 16-24.

Gaffen, D. J., and R. J. Ross (1998), Increased summertime heat stress in the US, *Nature*, *396*(6711), 529-530.

Gerten, D., S. Schaphoff, U. Haberlandt, W. Lucht, and S. Sitch (2004), Terrestrial vegetation and water balance - hydrological evaluation of a dynamic global vegetation model, *Journal of Hydrology*, *286*(1-4), 249-270.

Grell, G. A., and D. Devenyi (2002), A generalized approach to parameterizing convection combining ensemble and data assimilation techniques, *Geophys Res Lett*, *29*(14).

Guo, Z. C., et al. (2006), GLACE: The Global Land-Atmosphere Coupling Experiment. Part II: Analysis, *Journal of Hydrometeorology*, *7*(4), 611-625.

Hahn, G. L. (1999), Dynamic responses of cattle to thermal heat loads, *Journal of Animal Science*, *77*, 10-20.

Harding, K. J., and P. K. Snyder (2012), Modeling the Atmospheric Response to Irrigation in the Great Plains. Part I: General Impacts on Precipitation and the Energy Budget, *Journal of Hydrometeorology*, *13*, 1667-1686.

Hong, S. Y., Y. Noh, and J. Dudhia (2006), A new vertical diffusion package with an explicit treatment of entrainment processes, *Monthly Weather Review*, *134*(9), 2318-2341.

Howell, T. A., J. L. Hatfield, H. Yamada, and K. R. Davis (1984), Evaluation of Cotton Canopy Temperature to Detect Crop Water-Stress, *Transactions of the Asae*, *27*(1), 84-88.

IPCC (2007), IPCC Fourth Assessment Report: Climate Change 2007, *Rep.*

Jin, J. M., and N. L. Miller (2011), Regional simulations to quantify land use change and irrigation impacts on hydroclimate in the California Central Valley, *Theor Appl Climatol*, *104*(3-4), 429-442.

Jin, J. M., N. L. Miller, and N. Schlegel (2010), Sensitivity Study of Four Land Surface Schemes in the WRF Model, *Adv Meteorol*.

Jolly, W. M., M. Dobbertin, N. E. Zimmermann, and M. Reichstein (2005), Divergent vegetation growth responses to the 2003 heat wave in the Swiss Alps, *Geophys Res Lett*, *32*(18).

Kain, J. S. (2004), The Kain-Fritsch convective parameterization: An update, *Journal of Applied Meteorology*, *43*(1), 170-181.

Kalnay, E., and M. Cai (2003), Impact of urbanization and land-use change on climate, *Nature*, *423*(6939), 528-531.

Kanamitsu, M., W. Ebisuzaki, J. Woollen, S. K. Yang, J. J. Hnilo, M. Fiorino, and G. L. Potter (2002), Ncep-Doe Amip-Ii Reanalysis (R-2), *Bulletin of the American Meteorological Society*, *83*(11), 1631-1643.

Karoly, D. J., K. Braganza, P. A. Stott, J. M. Arblaster, G. A. Meehl, A. J. Broccoli, and K. W. Dixon (2003), Detection of a human influence on North American climate, *Science*, *302*(5648), 1200-1203.

Kenny, J. F., N. L. Barber, S. S. Hutson, K. S. Linsey, J. K. Lovelace, and M. A. Maupin (2005), Estimated Use of Water in the United States in 2005, *Rep.*, U.S. Department of the Interior

U.S. Geological Survey.

Kimball, B. A., and S. B. Idso (1983), Increasing Atmospheric Co2 - Effects on Crop Yield, Water-Use and Climate, *Agricultural Water Management*, *7*(1-3), 55-72.

Koster, R. D., et al. (2004), Regions of strong coupling between soil moisture and precipitation, *Science*, *305*(5687), 1138-1140.

Krinner, G., N. Viovy, N. de Noblet-Ducoudre, J. Ogee, J. Polcher, P. Friedlingstein, P. Ciais, S. Sitch, and I. C. Prentice (2005), A dynamic global vegetation model for studies of the coupled atmosphere-biosphere system, *Global Biogeochemical Cycles*, *19*(1).

Kucharik, C. J. (2003), Evaluation of a Process-Based Agro-Ecosystem Model (Agro-IBIS) across the US Corn Belt: Simulations of the Interannual Variability in Maize Yield, *Earth Interact*, *7*.

Kueppers, L. M., and M. A. Snyder (2012), Influence of irrigated agriculture on diurnal surface energy and water fluxes, surface climate, and atmospheric circulation in California, *Climate Dynamics*, *38*(5-6), 1017-1029.

Kueppers, L. M., M. A. Snyder, and L. C. Sloan (2007a), Irrigation cooling effect: Regional climate forcing by land-use change, *Geophysical Research Letters, **34**(**3**)*, L03703, doi: doi:10.1029/2006gl028679.

Kueppers, L. M., M. A. Snyder, and L. C. Sloan (2007b), Irrigation cooling effect: Regional climate forcing by land-use change, *Geophys Res Lett*, *34*(3).

Kunkel, K. E., S. A. Changnon, B. C. Reinke, and R. W. Arritt (1996), The July 1995 heat wave in the midwest: A climatic perspective and critical weather factors, *Bulletin of the American Meteorological Society*, *77*(7), 1507-1518.

Lal, R. (2004), Soil carbon sequestration impacts on global climate change and food security, *Science*, *304*(5677), 1623-1627.

Lascano, R. J., C. H. M. Vanbavel, J. L. Hatfield, and D. R. Upchurch (1987), Energy and Water-Balance of a Sparse Crop - Simulated and Measured Soil and Crop Evaporation, *Soil Science Society of America Journal*, *51*(5), 1113-1121.

Lawlor, D. W., and R. A. C. Mitchell (1991), The Effects of Increasing Co2 on Crop Photosynthesis and Productivity - a Review of Field Studies, *Plant Cell Environ*, *14*(8), 807-818.

Lawrence, D. M., P. E. Thornton, K. W. Oleson, and G. B. Bonan (2007), The partitioning of evapotranspiration into transpiration, soil evaporation, and canopy evaporation in a GCM: Impacts on land-atmosphere interaction, *Journal of Hydrometeorology*, *8*(4), 862-880.

Lawrence, D. M., K. W. Oleson, M. G. Flanner, C. G. Fletcher, P. J. Lawrence, S. Levis, S. C. Swenson, and G. B. Bonan (2012), The CCSM4 Land Simulation, 1850-2005: Assessment of Surface Climate and New Capabilities, *J Climate*, *25*(7), 2240-2260.

Lawrence, D. M., et al. (2011), Parameterization Improvements and Functional and Structural Advances in Version 4 of the Community Land Model, *J. Adv. Model. Earth Syst.* , *3*(M03001), 27.

Lawrence, P. J., and T. N. Chase (2007), Representing a new MODIS consistent land surface in the Community Land Model (CLM 3.0), *Journal of Geophysical Research-Biogeosciences, 112*(G1), G01023, doi: 10.1029/2006jg000168.

Levis, S., G. B. Bonan, E. Kluzek, P. E. Thornton, A. Jones, W. J. Sacks, and C. J. Kucharik (2012), Interactive Crop Management in the Community Earth System Model (CESM1): Seasonal Influences on Land-Atmosphere Fluxes, *Journal of Climate*, *25*(14), 4839-4859.

Liang, X. Z., M. Xu, W. Gao, K. R. Reddy, K. Kunkel, D. L. Schmoldt, and A. N. Samel (2012), A Distributed Cotton Growth Model Developed from GOSSYM and Its Parameter Determination, *Agron J*, *104*(3), 661-674.

Lin, Y. L., R. D. Farley, and H. D. Orville (1983), Bulk Parameterization of the Snow Field in a Cloud Model, *Journal of Climate and Applied Meteorology*, *22*(6), 1065-1092.

Lizaso, J. I., and J. T. Ritchie (1997), A modified version of CERES to predict the impact of soil water excess on maize crop growth and development, *Syst Appr S*, *6*, 153-167.

Lo, M. H., and J. S. Famiglietti (2013), Irrigation in California's Central Valley strengthens the southwestern U.S. water cycle, *Geophys Res Lett*, *40*(2), 301-306.

Lobell, D., G. Bala, A. Mirin, T. Phillips, R. Maxwell, and D. Rotman (2009), Regional Differences in the Influence of Irrigation on Climate, *J Climate*, *22*(8), 2248-2255.

Lobell, D. B., and C. B. Field (2007), Global scale climate - crop yield relationships and the impacts of recent warming, *Environ Res Lett*, *2*(1).

Lobell, D. B., C. J. Bonfils, L. M. Kueppers, and M. A. Snyder (2008a), Irrigation cooling effect on temperature and heat index extremes, *Geophys Res Lett*, *35*(9).

Lobell, D. B., M. B. Burke, C. Tebaldi, M. D. Mastrandrea, W. P. Falcon, and R. L. Naylor (2008b), Prioritizing climate change adaptation needs for food security in 2030, *Science*, *319*(5863), 607-610.

Long, S. P., E. A. Ainsworth, A. D. B. Leakey, J. Nosberger, and D. R. Ort (2006), Food for thought: Lower-than-expected crop yield stimulation with rising CO2 concentrations, *Science*, *312*(5782), 1918-1921.

Lu, L. X., R. A. Pielke, G. E. Liston, W. J. Parton, D. Ojima, and M. Hartman (2001), Implementation of a two-way interactive atmospheric and ecological model and its application to the central United States, *Journal of Climate*, *14*(5), 900-919.

Lu, Y. Q., and L. M. Kueppers (2012), Surface energy partitioning over four dominant vegetation types across the United States in a coupled regional climate model (Weather Research and Forecasting Model 3-Community Land Model 3.5), *Journal of Geophysical Research-Atmospheres*, *117*.

Lynch, A. H., F. S. Chapin, L. D. Hinzman, W. Wu, E. Lilly, G. Vourlitis, and E. Kim (1999), Surface energy balance on the arctic tundra: Measurements and models, *Journal of Climate*, *12*(8), 2585-2606.

Malhi, Y., J. T. Roberts, R. A. Betts, T. J. Killeen, W. H. Li, and C. A. Nobre (2008), Climate change, deforestation, and the fate of the Amazon, *Science*, *319*(5860), 169-172.

Markovic, M., C. G. Jones, P. A. Vaillancourt, D. Paquin, K. Winger, and D. Paquin-Ricard (2008), An evaluation of the surface radiation budget over North America for a suite of regional climate models against surface station observations, *Climate Dynamics*, *31*(7-8), 779-794.

Mearns, L. O., C. Rosenzweig, and R. Goldberg (1992), Effect of Changes in Interannual Climatic Variability on Ceres-Wheat Yields - Sensitivity and 2 X Co2 General-Circulation Model Studies, *Agr Forest Meteorol*, *62*(3-4), 159-189.

Mendelsohn, R., W. D. Nordhaus, and D. Shaw (1994), The Impact of Global Warming on Agriculture - a Ricardian Analysis, *Am Econ Rev*, *84*(4), 753-771.

Mlawer, E. J., S. J. Taubman, P. D. Brown, M. J. Iacono, and S. A. Clough (1997), Radiative transfer for inhomogeneous atmospheres: RRTM, a validated correlated-k model for the longwave, *Journal of Geophysical Research-Atmospheres*, *102*(D14), 16663-16682.

Moss, D. N. (1962), Limiting Carbon Dioxide Concentration for Photosynthesis, *Nature*, *193*(4815), 587-&.

Nakanishi, M., and H. Niino (2006), An improved mellor-yamada level-3 model: Its numerical stability and application to a regional prediction of advection fog, *Boundary-Layer Meteorology*, *119*(2), 397-407.

Nakanishi, M., and H. Niino (2009), Development of an Improved Turbulence Closure Model for the Atmospheric Boundary Layer, *Journal of the Meteorological Society of Japan*, *87*(5), 895-912.

Naughton, M. P., A. Henderson, M. C. Mirabelli, R. Kaiser, J. L. Wilhelm, S. M. Kieszak, C. H. Rubin, and M. A. McGeehin (2002), Heat-related mortality during a 1999 heat wave in Chicago, *American Journal of Preventive Medicine*, *22*(4), 221-227.

Nielsen, R. L. (2011), Field drydown of mature corn grain, [On-line], Available: http://www.agry.purdue.edu/ext/corn/news/timeless/graindrying.html

Niu, G. Y., and Z. L. Yang (2006), Effects of frozen soil on snowmelt runoff and soil water storage at a continental scale, *Journal of Hydrometeorology*, *7*(5), 937-952.

Niu, G. Y., Z. L. Yang, R. E. Dickinson, and L. E. Gulden (2005), A simple TOPMODEL-based runoff parameterization (SIMTOP) for use in global climate models, *Journal of Geophysical Research-Atmospheres, 110*(D21), D21106, doi: 10.1029/2005jd006111.

Niu, G. Y., Z. L. Yang, R. E. Dickinson, L. E. Gulden, and H. Su (2007), Development of a simple groundwater model for use in climate models and evaluation with Gravity Recovery and Climate Experiment data, *Journal of Geophysical Research-Atmospheres, 112*(D7), D07103, doi: 10.1029/2006jd007522.

Oleson, K. W., G. B. Bonan, S. Levis, and M. Vertenstein (2004), Effects of land use change on North American climate: impact of surface datasets and model biogeophysics, *Clim Dynam*, *23*(2), 117-132.

Oleson, K. W., et al. (2008), Improvements to the Community Land Model and their impact on the hydrological cycle, *Journal of Geophysical Research-Biogeosciences, 113*(G1), G01021, doi: 10.1029/2007jg000563.

Oleson, K. W., et al. (2010), Technical Description of version 4.0 of the Community Land Model (CLM), *Rep. ISSN Electronic Edition 2153-2400*, National Center for Atmospheric Research, Boulder, CO.

Osborne, T. M., D. M. Lawrence, A. J. Challinor, J. M. Slingo, and T. R. Wheeler (2007), Development and assessment of a coupled crop-climate model, *Global Change Biology*, *13*(1), 169-183.

Otterman, J. (1977), Anthropogenic Impact on Albedo of Earth, *Climatic Change*, *1*(2), 137-155.

Ozdogan, M., and G. D. Salvucci (2004), Irrigation-induced changes in potential evapotranspiration in southeastern Turkey: Test and application of Bouchet's complementary hypothesis, *Water Resour Res*, *40*(4).

Peiris, D. R., J. W. Crawford, C. Grashoff, R. A. Jefferies, J. R. Porter, and B. Marshall (1996), A simulation study of crop growth and development under climate change, *Agr Forest Meteorol*, *79*(4), 271-287.

Peiris, T. S. G., R. O. Thattil, and R. Mahindapala (1995), An Analysis of the Effect of Climate and Weather on Coconut (Cocos-Nucifera), *Exp Agr*, *31*(4), 451-460.

Pessarakli, M. (1999), *Handbook of plant and crop stress*, Marcel Dekker, Inc., New York.

Pielke, R. A., G. Marland, R. A. Betts, T. N. Chase, J. L. Eastman, J. O. Niles, D. D. S. Niyogi, and S. W. Running (2002), The influence of land-use change and landscape dynamics on the climate system: relevance to climate-change policy

beyond the radiative effect of greenhouse gases, *Philosophical Transactions of the Royal Society of London Series a-Mathematical Physical and Engineering Sciences*, *360*(1797), 1705-1719.

Pielke, R. A., J. Adegoke, A. Beltran-Przekurat, C. A. Hiemstra, J. Lin, U. S. Nair, D. Niyogi, and T. E. Nobis (2007), An overview of regional land-use and land-cover impacts on rainfall, *Tellus Series B-Chemical and Physical Meteorology*, *59*(3), 587-601.

Pitman, A., R. Pielke, R. Avissar, M. Claussen, J. Gash, and H. Dolman (1999), The role of the land surface in weather and climate: Does the land surface matter?. *Int. Geophere Biosphere Programme News Letter*, *39*, 4-11.

Porter, J. R., and M. A. Semenov (2005), Crop responses to climatic variation, *Philos T Roy Soc B*, *360*(1463), 2021-2035.

Raschke, E., A. Ohmura, W. B. Rossow, B. E. Carlson, Y. C. Zhang, C. Stubenrauch, M. Kottek, and M. Wild (2005), Cloud effects on the radiation budget based on ISCCP data (1991 to 1995), *International Journal of Climatology*, *25*(8), 1103-1125.

Reusch, T. B. H., A. Ehlers, A. Hammerli, and B. Worm (2005), Ecosystem recovery after climatic extremes enhanced by genotypic diversity, *Proceedings of the National Academy of Sciences of the United States of America*, *102*(8), 2826-2831.

Ritchie, J. R., and S. Otter (1985), Description and performance of CERES-Wheat: a user-oriented wheat yield model, *ARS - United States Department of Agriculture, Agricultural Research Service*, *38*, 159-175.

Rosenberg, N. J. (1982), The Increasing Co2 Concentration in the Atmosphere and Its Implication on Agricultural Productivity .2. Effects through Co2-Induced Climatic-Change, *Climatic Change*, *4*(3), 239-254.

Rosenberg, N. J., M. S. Mckenney, W. E. Easterling, and K. M. Lemon (1992), Validation of Epic Model Simulations of Crop Responses to Current Climate and Co2 Conditions - Comparisons with Census, Expert Judgment and Experimental Plot Data, *Agr Forest Meteorol*, *59*(1-2), 35-51.

Rosenzweig, C., and M. L. Parry (1994), Potential Impact of Climate-Change on World Food-Supply, *Nature*, *367*(6459), 133-138.

Sacks, W. J., D. Deryng, J. A. Foley, and N. Ramankutty (2010), Crop planting dates: an analysis of global patterns, *Global Ecol Biogeogr*, *19*(5), 607-620.

Sacks, W. J., B. I. Cook, N. Buenning, S. Levis, and J. H. Helkowski (2009), Effects of global irrigation on the near-surface climate, *Climate Dynamics*, *33*(2-3), 159-175.

Saeed, F., S. Hagemann, and D. Jacob (2009), Impact of irrigation on the South Asian summer monsoon, *Geophys Res Lett*, *36*.

Sakaguchi, K., and X. B. Zeng (2009), Effects of soil wetness, plant litter, and under-canopy atmospheric stability on ground evaporation in the Community Land Model (CLM3.5), *Journal of Geophysical Research-Atmospheres*, *114*, -.

Sampaio, G., C. Nobre, M. H. Costa, P. Satyamurty, B. S. Soares, and M. Cardoso (2007), Regional climate change over eastern Amazonia caused by pasture and soybean cropland expansion, *Geophys Res Lett*, *34*(17).

Scanlon, B. R., C. C. Faunt, L. Longuevergne, R. C. Reedy, W. M. Alley, V. L. McGuire, and P. B. McMahon (2012), Groundwater depletion and sustainability of irrigation in the US High Plains and Central Valley, *Proceedings of the National Academy of Sciences of the United States of America*, *109*(24), 9320-9325.

Schmid, H. P., H. B. Su, C. S. Vogel, and P. S. Curtis (2003), Ecosystem-atmosphere exchange of carbon dioxide over a mixed hardwood forest in northern lower Michigan, *Journal of Geophysical Research-Atmospheres, 108*(D14), 4417, doi: 10.1029/2002jd003011.

Schoen, C. (2005), A new empirical model of the temperature-humidity index, *Journal of Applied Meteorology*, *44*(9), 1413-1420.

Searchinger, T., R. Heimlich, R. A. Houghton, F. X. Dong, A. Elobeid, J. Fabiosa, S. Tokgoz, D. Hayes, and T. H. Yu (2008), Use of US croplands for biofuels increases greenhouse gases through emissions from land-use change, *Science*, *319*(5867), 1238-1240.

Sellers, P. J., M. D. Heiser, and F. G. Hall (1992), Relations between Surface Conductance and Spectral Vegetation Indexes at Intermediate (100m2 to 15km2) Length Scales, *Journal of Geophysical Research-Atmospheres*, *97*(D17), 19033-19059.

Semenza, J. C., C. H. Rubin, K. H. Falter, J. D. Selanikio, W. D. Flanders, H. L. Howe, and J. L. Wilhelm (1996), Heat-related deaths during the July 1995 heat wave in Chicago, *New England Journal of Medicine*, *335*(2), 84-90.

Seneviratne, S. I., D. Luthi, M. Litschi, and C. Schar (2006), Land-atmosphere coupling and climate change in Europe, *Nature*, *443*(7108), 205-209.

Shukla, J., C. Nobre, and P. Sellers (1990), Amazon Deforestation and Climate Change, *Science*, *247*(4948), 1322-1325.

Siebert, S., P. Doll, J. Hoogeveen, J. M. Faures, K. Frenken, and S. Feick (2005), Development and validation of the global map of irrigation areas, *Hydrology and Earth System Sciences*, *9*(5), 535-547.

Sitch, S., et al. (2003), Evaluation of ecosystem dynamics, plant geography and terrestrial carbon cycling in the LPJ dynamic global vegetation model, *Global Change Biology*, *9*(2), 161-185.

Skamarock, W. C., J. B. Klemp, J. Dudhia, D. O. Gill, D. M. Barker, M. G. Duda, X. Huang, W. Wang, and J. G. Powers (2008), A description of the Advanced Research WRF Version 3, *Rep. NCAR/TN-475+STR*, National Center for Atmospheric Research, Boulder, CO.

Smoyer, K. E. (1998), A comparative analysis of heat waves and associated mortality in St. Louis, Missouri - 1980 and 1995, *International Journal of Biometeorology*, *42*(1), 44-50.

Sorooshian, S., J. L. Li, K. L. Hsu, and X. G. Gao (2011), How significant is the impact of irrigation on the local hydroclimate in California's Central Valley? Comparison of model results with ground and remote-sensing data, *J Geophys Res-Atmos*, *116*.

Steadman, R. G. (1984), A Universal Scale of Apparent Temperature, *Journal of Climate and Applied Meteorology*, *23*(12), 1674-1687.

Stockli, R., D. M. Lawrence, G. Y. Niu, K. W. Oleson, P. E. Thornton, Z. L. Yang, G. B. Bonan, A. S. Denning, and S. W. Running (2008), Use of FLUXNET in the

community land model development, *Journal of Geophysical Research-Biogeosciences, 113*(G1), G01025, doi: 10.1029/2007jg000562.

Stott, P. A., D. A. Stone, and M. R. Allen (2004), Human contribution to the European heatwave of 2003, *Nature*, *432*(7017), 610-614.

Su, W. Y., A. Bodas-Salcedo, K. M. Xu, and T. P. Charlock (2010), Comparison of the tropical radiative flux and cloud radiative effect profiles in a climate model with Clouds and the Earth's Radiant Energy System (CERES) data, *Journal of Geophysical Research-Atmospheres, 115*, D01105, doi: 10.1029/2009jd012490.

Subin, Z. M., W. J. Riley, J. Jin, D. S. Christianson, M. S. Torn, and L. M. Kueppers (2011), Ecosystem Feedbacks to Climate Change in California: Development, Testing, and Analysis Using a Coupled Regional Atmosphere and Land Surface Model (WRF3-CLM3.5), *Earth Interactions*, *15*.

Tawfik, A. B., and A. L. Steiner (2011), The role of soil ice in land-atmosphere coupling over the United States: A soil moisture-precipitation winter feedback mechanism, *Journal of Geophysical Research-Atmospheres*, *116*.

Tett, S. F. B., P. A. Stott, M. R. Allen, W. J. Ingram, and J. F. B. Mitchell (1999), Causes of twentieth-century temperature change near the Earth's surface, *Nature*, *399*(6736), 569-572.

Thompson, G., R. M. Rasmussen, and K. Manning (2004), Explicit forecasts of winter precipitation using an improved bulk microphysics scheme. Part I: Description and sensitivity analysis, *Monthly Weather Review*, *132*(2), 519-542.

Thompson, G., P. R. Field, R. M. Rasmussen, and W. D. Hall (2008), Explicit Forecasts of Winter Precipitation Using an Improved Bulk Microphysics Scheme. Part II: Implementation of a New Snow Parameterization, *Monthly Weather Review*, *136*(12), 5095-5115.

Thornton, P. E., and N. E. Zimmermann (2007), An improved canopy integration scheme for a land surface model with prognostic canopy structure, *Journal of Climate*, *20*(15), 3902-3923.

Tsvetsinskaya, E., L. O. Mearns, and W. E. Easterling (2000), Effects of plant growth and development on interannaul variability in mesoscale atmospheric simulations, *Proceedings of the 10th (2000) International Offshore and Polar Engineering Conference, Vol I*, 729-736.

van der Velde, M., G. Wriedt, and F. Bouraoui (2010), Estimating irrigation use and effects on maize yield during the 2003 heatwave in France, *Agr Ecosyst Environ*, *135*(1-2), 90-97.

Wagenvoort, W. A., and J. F. Bierhuizen (1977), Some Aspects of Seed-Germination in Vegetables .2. Effect of Temperature-Fluctuation, Depth of Sowing, Seed Size and Cultivar, on Heat Sum and Minimum Temperature for Germination, *Scientia Horticulturae*, *6*(4), 259-270.

Walker, M. D., and N. S. Diffenbaugh (2009), Evaluation of high-resolution simulations of daily-scale temperature and precipitation over the United States, *Climate Dynamics*, *33*(7-8), 1131-1147.

Wanjura, D. F., D. R. Upchurch, and J. R. Mahan (1992), Automated Irrigation Based on Threshold Canopy Temperature, *Transactions of the Asae*, *35*(5), 1411-1417.

Wielicki, B. A., B. R. Barkstrom, E. F. Harrison, R. B. Lee, G. L. Smith, and J. E. Cooper (1996), Clouds and the earth's radiant energy system (CERES): An earth

observing system experiment, *Bulletin of the American Meteorological Society*, *77*(5), 853-868.

Wild, M. (2008), Short-wave and long-wave surface radiation budgets in GCMs: a review based on the IPCC-AR4/CMIP3 models, *Tellus Series a-Dynamic Meteorology and Oceanography*, *60*(5), 932-945.

Wild, M., and E. Roeckner (2006), Radiative fluxes in the ECHAM5 general circulation model, *Journal of Climate*, *19*(16), 3792-3809.

Wild, M., A. Ohmura, H. Gilgen, J. J. Morcrette, and A. Slingo (2001), Evaluation of downward longwave radiation in general circulation models, *Journal of Climate*, *14*(15), 3227-3239.

Wilkerson, G. G., J. W. Jones, K. J. Boote, K. T. Ingram, and J. W. Mishoe (1983), Modeling Soybean Growth for Crop Management, *T Asae*, *26*(1), 63-73.

Williams, M., et al. (2009), Improving land surface models with FLUXNET data, *Biogeosciences*, *6*(7), 1341-1359.

Wilson, K., et al. (2002a), Energy balance closure at FLUXNET sites, *Agricultural and Forest Meteorology*, *113*(1-4), 223-243.

Wilson, K. B., et al. (2002b), Energy partitioning between latent and sensible heat flux during the warm season at FLUXNET sites, *Water Resources Research*, *38*(12), 1294.

Wilson, T. B., and T. P. Meyers (2007), Determining vegetation indices from solar and photosynthetically active radiation fluxes, *Agricultural and Forest Meteorology*, *144*(3-4), 160-179.

Wise, R. R., A. J. Olson, S. M. Schrader, and T. D. Sharkey (2004), Electron transport is the functional limitation of photosynthesis in field-grown Pima cotton plants at high temperature, *Plant Cell and Environment*, *27*(6), 717-724.

Wofsy, S. C., and D. Y. Hollinger (1998), Science Plan for AmeriFlux: Long-term flux measurement network of the Americas
, Nat'l Inst. for Global Envir. Change (NIGEC), [On-line], Available: http://public.ornl.gov/ameriflux/docs/scif.doc

Xu, M., X.-Z. Liang, W. Gao, K. R. Reddy, J. Slusser, and K. Kunkel (2005), Preliminary results of the coupled CWRF-GOSSYM system,
Remote Sensing and Modeling of Ecosystems for Sustainability II, *5884*.

Yang, W. Z., et al. (2006), MODIS leaf area index products: From validation to algorithm improvement, *Ieee Transactions on Geoscience and Remote Sensing*, *44*(7), 1885-1898.

Young, D. F., P. Minnis, D. R. Doelling, G. G. Gibson, and T. Wong (1998), Temporal interpolation methods for the Clouds and the Earth's Radiant Energy system (CERES) experiment, *Journal of Applied Meteorology*, *37*(6), 572-590.

Zeng, X. B. (2001), Global vegetation root distribution for land modeling, *Journal of Hydrometeorology*, *2*(5), 525-530.

Zhu, Z., J. Bi, Y. Pan, S. Ganguly, A. Anav, L. Xu, A. Samanta, S. Piao, R. R. Nemani, and R. B. Myneni (2012), Global Data Sets of Vegetation LAI3g and FPAR3g derived from GIMMS NDVI3g for the period 1981 to 2011, *Remote Sensing*, *4*.

APPENDIX A

Dynamic crop module in WRF3.3-CLM4crop

We incorporated the dynamic crop growth module from CLM4CNCrop into the coupled regional model WRF3.3-CLM4. The dynamic crop growth module is based on AgroIBIS [*Kucharik*, 2003], is described in detail in Levis et al. (2012) and is summarized in this appendix.

A1. Modifications

We made several modifications to the dynamic crop module to better fit the coupled regional model framework. First, we fixed the soil carbon and nitrogen state variables. In the original CLM4CNCrop model, crop growth is linked to the carbon and nitrogen model, which updates multiple soil and plant carbon and nitrogen variables at each time step based on crop phenology and environmental changes. It requires a long spin-up time (over thousands of years) to enable the soil carbon and nitrogen to reach current steady states. For a high-resolution regional climate model, such long spin-up simulations are difficult with current computing resources. Further, even though soil carbon and nitrogen are simulated in CLM4CNCrop, these values would not be routinely coupled to atmospheric carbon and nitrogen in a regional model. Since our regional scale focus is on biogeophysical, not biogeochemical feedbacks, between land and atmosphere, we assumed that for crops, the soil carbon and nitrogen could be maintained at optimum levels year to year.

Second, at this stage, we consider WRF3.3-CLM4crop able to simulate C3 and C4 crops, not more specific crop types. The current version of CLM4CNCrop simulates three crops (summer cereal, soybean, corn). The growth of these crops is strongly dependent on photosynthetic pathway. We assume that at a regional scale, it's inappropriate to expect the model to simulate specific crops across the domain with validation only at one or several grid cells where observations are available. Therefore, we used C3 and C4 crop types to represent the potential growth of major crops (e.g., C3 crops: wheat, soybean, and C4 crops: corn, sorghum). The next phase of our work will aim to gather more observations and validate growth parameters for more specific crop types.

Third, we made changes to crop phenology and carbon allocation to better suit the regional coupled model framework and applications. In the planting phase, we changed the 20-year running mean growing degree days into 5-year running mean growing degree days to better match our simulation period. In the harvest phase, we assumed harvest occurs when the crop reaches 1.5 times the GDD required for maturity rather than occurring as soon as the crop reaches maturity as in CLM4CNCrop, since some crops such as corn [*Nielsen*, 2011] are left in the field after maturity to dry. We also modified the carbon allocation to better reflect environmental stress on crop growth as described in section A3 of the appendix.

A2. Phenology

Planting

The thresholds for planting, and thus initiation of the crop development cycle, are defined as:

$$\begin{aligned} T_{2m} &> T_p \\ GDD_8 &> GDD_{\min} \end{aligned} \tag{1}$$

Where T_{2m} is the instantaneous 2-meter air temperature (°C), T_p is a crop-specific planting temperature (7°C for C3 crop and 10°C for C4 crop), GDD_8 is the 5-year running averaged growing degree days (base 8 °C) from March to September, and $GDD_{\min}$ is the minimum growing degree day requirement (50 degree days for both C3 and C4 crops). C3 crop must meet the planting temperature requirement between March 1st and May 14th , and C4 crop between May 1st and June 14th .

At planting, some initial values are assigned, including leaf area index (0.1 m^2/m^2), stem area index (0.01 m^2/m^2), leaf carbon (3 gC/m^2), stem carbon (3 gC/m^2), and fine root carbon (4.5 gC/m2). The growing degree day value necessary for the crop to reach vegetative and physiological maturity, GDD_{mat}, is updated:

$$\begin{aligned} GDD_{mat}^{c3crop} &= 0.85GDD_8 \\ GDD_{mat}^{c4crop} &= 0.85GDD_{10} \\ GDD_8 &= GDD_8 + T_{2m} - 8 \quad , \quad 0 \le T_{2m} - 8 \le 30^o days \\ GDD_{10} &= GDD_{10} + T_{2m} - 10 \quad , \quad 0 \le T_{2m} - 10 \le 30^o days \end{aligned} \tag{2}$$

where GDD_{10} is the 5-year running averaged growing degree days from March to September.

Leaf emergence

Leaves emerge when the growing degree days for soil temperature (0.05m depth soil, third layer of CLM) since planting ($GDD_{T_{soi}}$, base 0°C and 8°C for C3 and C4 crop) reaches 3% of GDD_{mat}. At this phase, available carbon is allocated to leaf, live stem, and fine root according to constant allocation coefficients. Leaf area index generally increase and reach a maximum value, which is prescribed as 6 $m^2.m^{-2}$ for C3 and 5 $m^2.m^{-2}$ for C4 crop. And the stem area index is updated as stem carbon gain or loss.

Grain fill

Grain begins to fill when the growing degree days since planting (GDD_{plant}) reaches 70% for C3 and 65% for C4 crop of GDD_{mat}. The leaf area index and stem area index decline and transfer some amount (defined in A3) of leaf and live stem carbon to grain.

Harvest

We assumed harvest occurs when the crop reaches 1.5 times the GDD required for maturity ($GDD_{plant} > 1.5GDD_{mat}$) rather than as soon as the crop reaches maturity as defined in CLM4CNCrop, since crops, such as corn were left in the field after maturity to dry [*Nielsen*, 2011]

A3. CN Allocation

Initial leaf carbon and nitrogen is assigned at planting. We adjusted the value from 1gC/m^2 in CLM4CNCrop to 3 gC/m^2 because the small initial leaf carbon generated a too small leaf carbon, resulting in low LAI compared to observations and too little Gross Primary Production (GPP) for carbon allocation. The initial leaf nitrogen was calculated using leaf C:N ratio from Levis et al. (2012). C and N allocation starts with leaf emergence and ends with harvest. Carbon allocation is based on allocation coefficients and the nitrogen is assigned based on the tissue (leaf, stem, root, and grain) C:N ratio.

Leaf emergence to grain fill

The allocation coefficients to each C pool are defined as:

$$\begin{aligned} a_{grain} &= 0 \\ a_{froot} &= 0.7(1-\beta_p) \\ a_{leaf} &= 0.5(1-a_{froot}) \\ a_{livestem} &= 0.5(1-a_{froot}) \end{aligned} \tag{3}$$

β_p is a plant functional type dependent variable that indicates the root water stress and varies from near zero (dry soil) to one (wet soil). We used β_p to better inform carbon allocation between root and shoot. When the soil is dry (small β_p), more carbon is allocated to the root [*Ericsson et al.*, 1996] to a maximum of 0.7. The rest of the available carbon is allocated to leaf and live stem in equal amounts.

Grain fill to harvest

During the grain filling period, fine root carbon allocation is still controlled by β_p, while the maximum C allocation to fine root is changed to 0.2. 80% of the remaining carbon is allocated to grain and the other 20% to tissues that are not explicitly simulated in the model, such as corn silk, flowers, etc. We assume the leaf and live stem carbon decline in this stage, and some portion of the carbon is transferred to grain.

$$
\begin{aligned}
a_{froot} &= 0.2(1-\beta_p) \\
a_{grain} &= 0.8(1-a_{froot}) \\
a_{leaf} &= 0 \\
a_{livestem} &= 0 \\
tran &= c_{timestep}(\tan\frac{GDD_{plant}}{GDD_p})
\end{aligned}
\tag{4}
$$

where *tran* is the transfer coefficient of leaf and live stem carbon to grain carbon, $c_{timestep}$ is an adjusted coefficient for each timestep, GDD_{plant} is the soil growing degree days since planting (base 8 °C for C3 crop and 10 °C for C4 crop), and GDD_p is the 5-year running averaged soil growing degree days from April to September (base 8 °C for C3 crop and 10 °C for C4 crop).

APPENDIX B

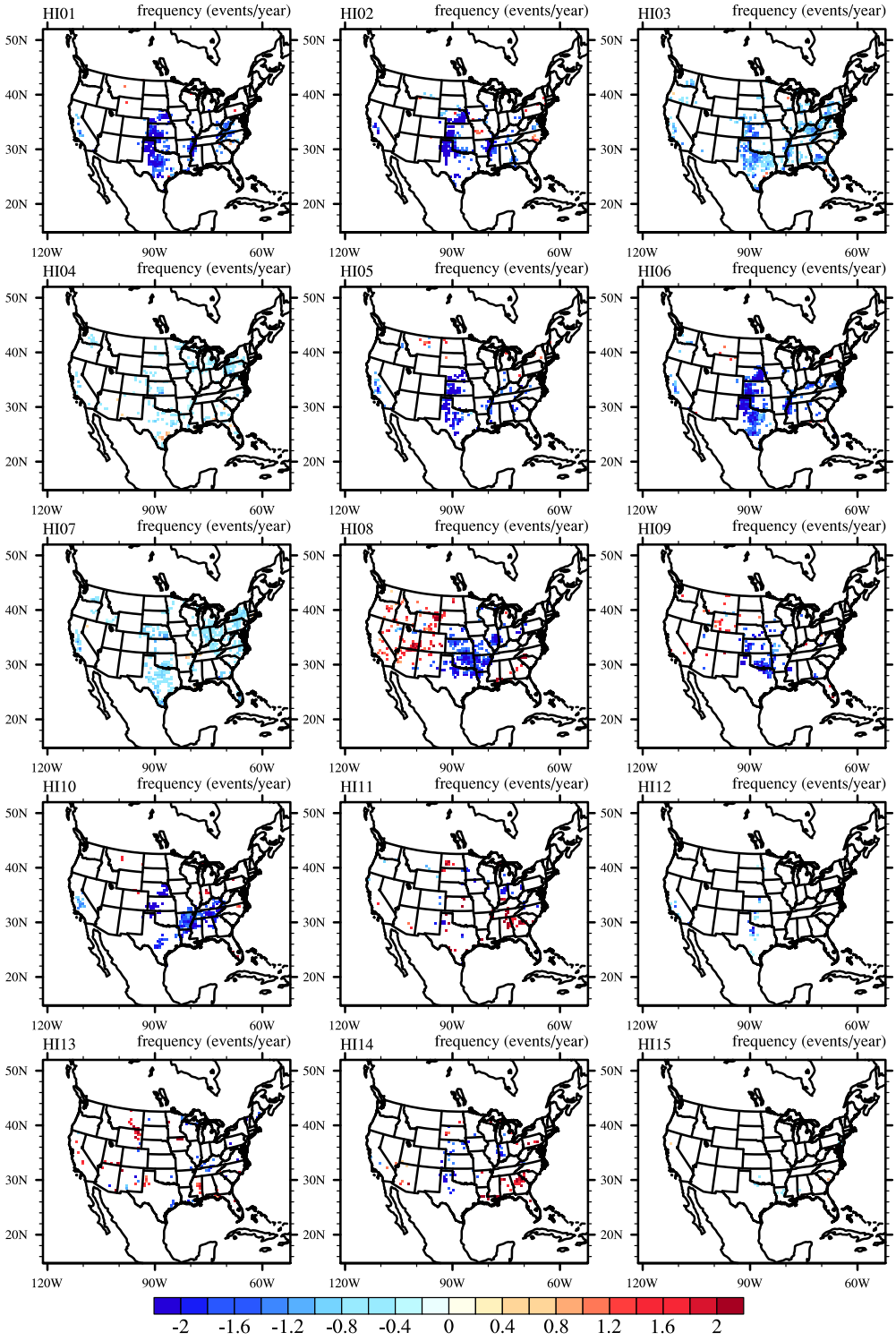

Figure S1. The 8-year (2004-2011) averaged significant difference (CROPIRR-CROP) of heat wave frequency for fifteen heat wave indices.

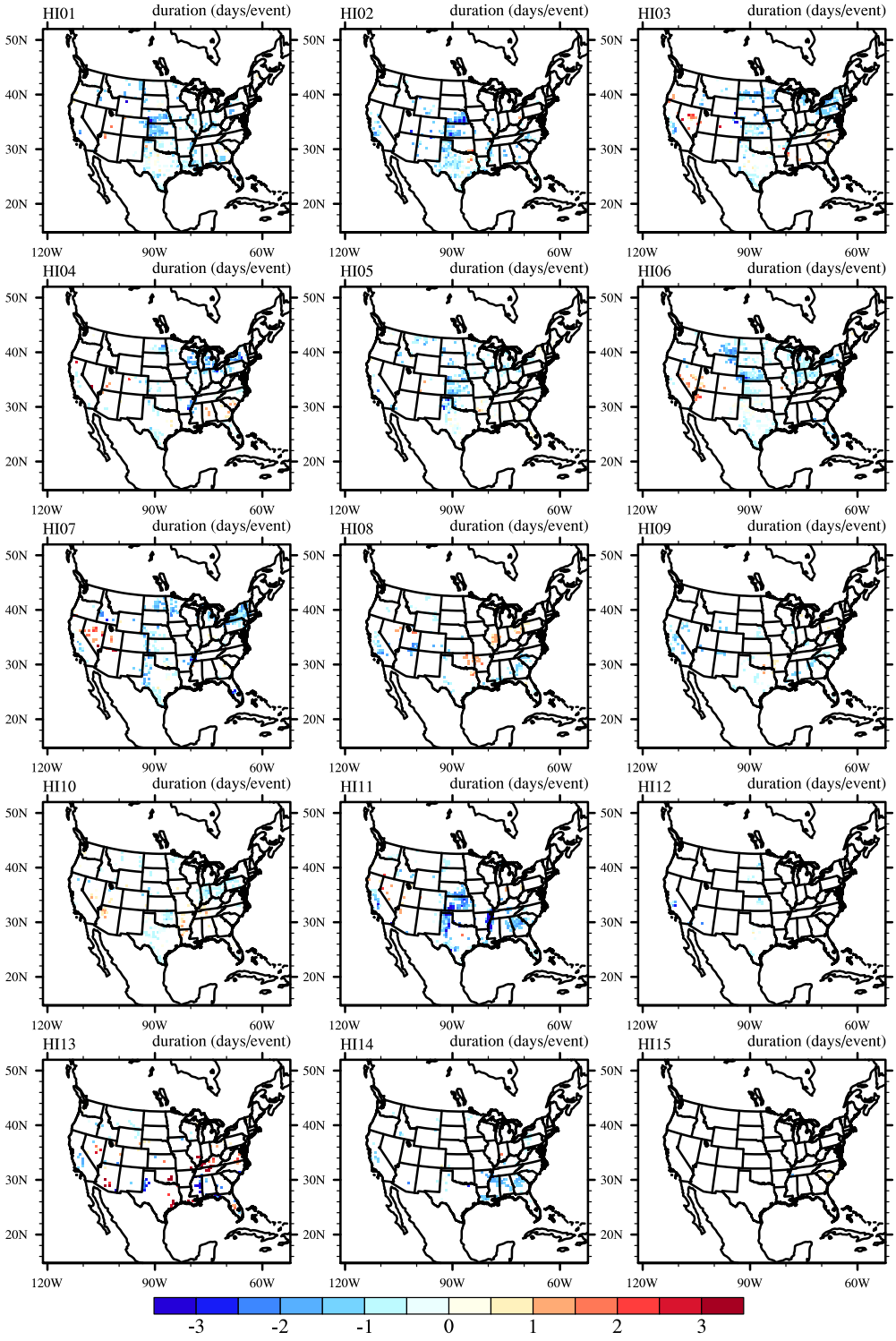

Figure S2. The 8-year (2004-2011) averaged significant difference (CROPIRR-CROP) of heat wave duration for fifteen heat wave indices.

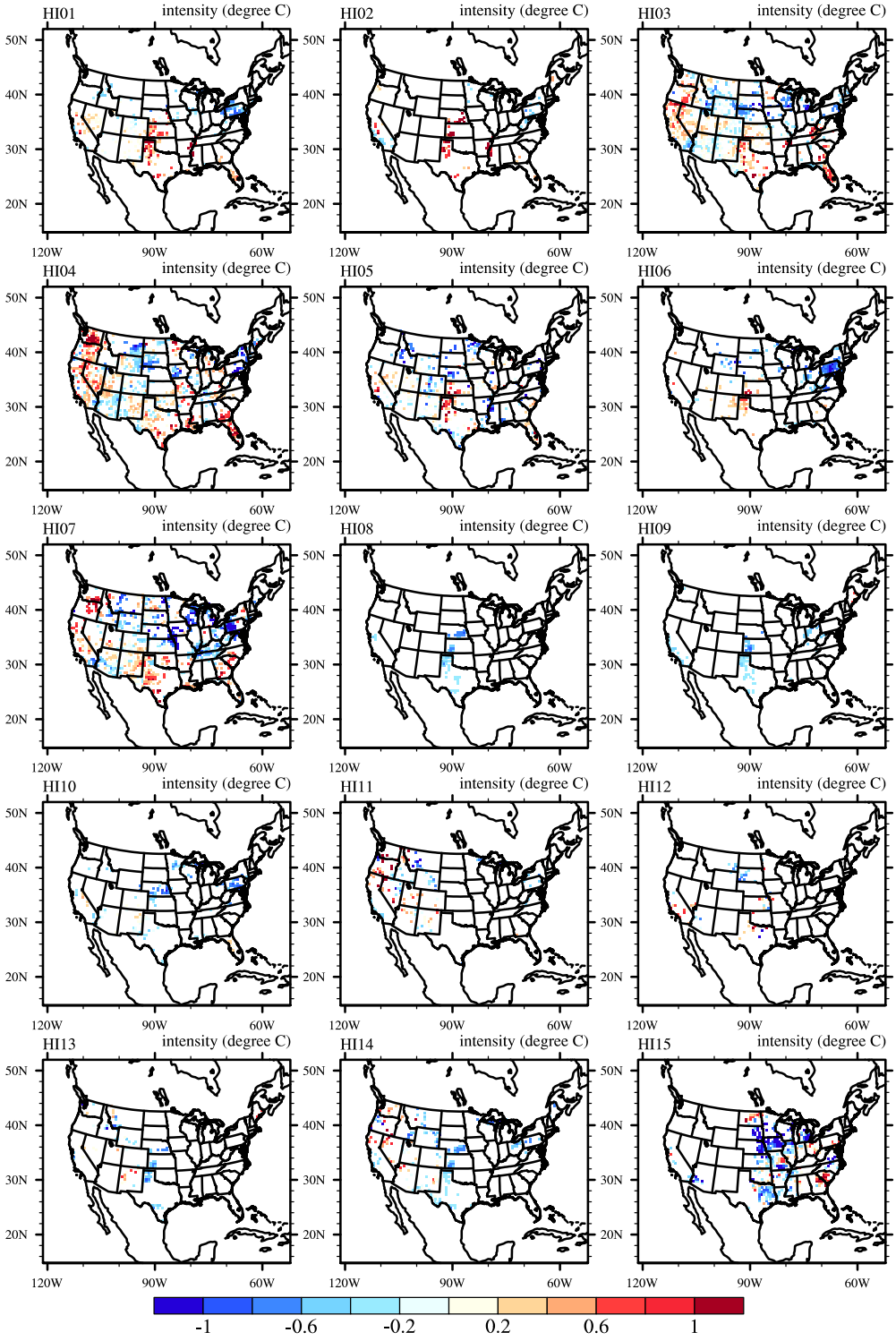

Figure S3. The 8-year (2004-2011) averaged significant difference (CROPIRR-CROP) of heat wave intensity for fifteen heat wave indices.

Heat Wave Indices	Temperature Metric	Threshold	Duration	HI Type
HI01	Mean daily temperature	>95th percentile	2+ consecutive days	Relative
HI02	Mean daily temperature	>90th percentile	2+ consecutive days	Relative
HI03	Mean daily temperature	>98th percentile	2+ consecutive days	Relative
HI04	Mean daily temperature	>99th percentile	2+ consecutive days	Relative
HI05	Minimum daily temperature	>95th percentile	2+ consecutive days	Relative
HI06	Maximum daily temperature	>95th percentile	2+ consecutive days	Relative
HI07	Maximum daily temperature	T1: >81st percentile T2: >97.5th percentile	Everyday, >T1; 3+ consecutive days, >T2; Avg Tmax> T1 for whole time period	Relative
HI08	Maximum daily apparent temperature	>85th percentile	1 day	Relative
HI09	Maximum daily apparent temperature	>90th percentile	1 day	Relative
HI10	Maximum daily apparent temperature	>95th percentile	1 day	Relative
HI11	Maximum daily temperature	>35^{o}C	1 day	Absolute
HI12	Minimum & maximum daily temperature	T_{min}>26.7 ^{o}C T_{max}>40.6 ^{o}C	≥1 threshold for 2+ consecutive days	Absolute
HI13	Maximum daily heat index	>80 ^{o}F	1 day	Absolute
HI14	Maximum daily heat index	>90 ^{o}F	1 day	Absolute
HI15	Maximum daily heat index	> 105 ^{o}F	1 day	Absolute

Table S1. The fifteen heat wave indices definition adopted from Smith et al., (2013), table 1.